Dual genetic tracing system identifies diverse and dynamic origins of cardiac valve mesenchyme

Kuo Liu[1,2], Wei Yu[1,2], Muxue Tang[3], Juan Tang[1,2], Xiuxiu Liu[1], Qiaozhen Liu[1,2], Yan Li[1,2], Lingjuan He[1,2], Libo Zhang[1,2], Sylvia M. Evans[5], Xueying Tian[4*], Kathy O. Lui[6], Bin Zhou[1,2,4,7*]

[1]The State Key Laboratory of Cell Biology, CAS Center for Excellence in Molecular Cell Science, Shanghai Institute of Biochemistry and Cell Biology, Chinese Academy of Sciences, University of Chinese Academy of Sciences, Shanghai, 200031, China.

[2]Key Laboratory of Nutrition and Metabolism, Institute for Nutritional Sciences, Shanghai Institutes for Biological Sciences, University of Chinese Academy of Sciences, Chinese Academy of Sciences, Shanghai, 200031, China.

[3]School of Life Sciences, East China Normal University, Shanghai, 200241, China.

[4]Key Laboratory of Regenerative Medicine of Ministry of Education, Jinan University, Guangzhou, 510632, China.

[5]Skaggs School of Pharmacy and Pharmaceutical Sciences, University of California at San Diego, La Jolla, CA 92093, USA.

[6]Department of Chemical Pathology; Li Ka Shing Institute of Health Sciences, The Chinese University of Hong Kong, Prince of Wales Hospital, Shatin, Hong Kong SAR, China.

[7]School of Life Science and Technology, ShanghaiTech University, Shanghai, 201210, China.

*Authors for correspondence: Xueying Tian[a], Bin Zhou[b]

[a]E-mail: xytianjnu@163.com

[b]E-mail: zhoubin@sibs.ac.cn

ABSTRACT

In vivo genomic engineering is instrumental for studying developmental biology and regenerative medicine. Development of novel systems with more site-specific recombinases (SSRs) that complement with the commonly used Cre-loxP would be valuable for more precise lineage tracing and genome editing. Here we introduce a new SSR system via Nigri-nox. By generating tissue-specific Nigri knock-in and its responding nox reporter mice, we show that Nigri-nox system works efficiently *in vivo* by targeting specific tissues. As a new orthogonal system to Cre-loxP, Nigri-nox provides an additional control of genetic manipulation. We also demonstrate how the two orthogonal systems Nigri-nox and Cre-loxP could be used simultaneously to map the cell fate of two distinct developmental origins of cardiac valve mesenchyme in the mouse heart, providing dynamics of cellular contribution from different origins for cardiac valve mesenchyme during development. This work provides a proof-of-principle application of the Nigri-nox system for *in vivo* mouse genomic engineering. Coupled with other SSR systems, Nigri-nox would be valuable for more precise delineation of origins and cell fates during development, diseases and regeneration.

KEY WORDS: Genetic engineering, Site-specific recombinase (SSR), Nigri-nox, Fate mapping, Cardiac valve development

INTRODUCTION

Precise genetic manipulation of cells *in vivo* advances our understanding of organ development and tissue regeneration. The widely used DNA site specific recombinase (SSR), Cre recombinase, allows predictable and efficient genomic modifications in Cre-expressing cells and their descendants, providing a powerful tool for genetic lineage tracing and gene manipulation *in vivo* (Buckingham and Meilhac, 2011; Kretzschmar and Watt, 2012). Nevertheless, Cre is usually driven by a single gene promoter so as to target one cell population during development, diseases or regeneration (Sauer and Henderson, 1988). By Cre-loxP recombination, the conventional single-colored loxP reporter system, such as *Rosa26-LacZ*, *Rosa26-tdTomato* or *Rosa26-GFP*, can be used to label Cre-expressing cells and their descendants (Soriano, 1999; Srinivas et al., 2001; Madisen et al., 2010). Although multicolor reporter systems have also been used for single cell clonal analysis such as Brainbow or Confetti (Livet et al., 2007; Snippert et al., 2010) and double markers (MADM) system (Devine et al., 2014), such a lineage tracing strategy still falls within the Cre-expressing cell population defined by a specific gene promoter. To achieve genetic targeting of two or more distinct cell populations *in vivo*, other SSR systems that are orthogonal to the conventional Cre-loxP based system should be explored for genetic engineering. Indeed, several SSR systems other than Cre-loxP have been identified, such as Flpe-Frt or Dre-rox (Rodriguez et al., 2000; Anastassiadis et al., 2009). Moreover, different SSR systems have been simultaneously used for more precise genomic engineering, such as intersectional genetics, sequential genetics or exclusive genetics (Jensen et al., 2008; Fenno et al., 2014; Schonhuber et al., 2014; He et al., 2017), allowing better understanding of cellular and molecular mechanisms *in vivo*.

Nigri-nox is a newly discovered SSR system, in which Nigri recombinase targets its own recombination DNA site nox (Karimova et al., 2016). The Sequence identity (ID) and similarity (SIM) of Nigri with respect to Cre are 17% and 25%, respectively, while the ID and SIM of Dre with respect to Cre are 39% and 49%. The lower ID and SIM may indicate the lesser cross talk between those two systems. (Karimova et al., 2016). For recombination sites, nox is about 35% similar to loxP by DNA sequences. Moreover, *in vitro* cell experiments show that Nigri specifically and efficiently recombines its target site nox but not loxP (Karimova et al., 2016). Moreover, Nigri-nox recombination has high efficiency and specificity without cross-recombining with other known SSR systems by *in vitro* experiments. The new reported Nigri-nox is orthogonal to the present Cre-loxP, Flp-frt and Dre-rox. These data indicate that the Nigri-nox system could be utilized with other SSR systems for more precise *in vivo* genomic engineering and genetic manipulation of specific cell population.

To explore if the Nigri-nox system could be used *in vivo*, we generated a *Cdh5-Nigri* mouse allele and tested *in vivo* to address whether Nigri-nox

recombination efficiently and specifically targets endothelial cells and their descendants. We generated a new reporter that allows either Cre-loxP or Nigri-nox recombination on the Rosa26 locus. Using this reporter line coupled with tissue specific Cre and Nigri recombinases, we simultaneously and genetically targeted two distinct progenitor cells in development and followed their cell fates with distinct lineage tracing reporters. Taking cardiac valve mesenchyme formation as an example, we traced different developmental origins for mesenchymal cells in cardiac valves of the developing heart. Dual lineage tracing of endocardial cells and epicardial cells showed their dynamic cell replacement in part of tricuspid and mitral valves from early to late embryonic development. Furthermore, we also used Nigri-nox and Cre-loxP systems to simultaneously trace the cell fate of endocardial cells and neural crest cells in the same mouse heart. We provided detailed dynamics of mesenchymal components from distinct developmental origins by using these two orthogonal systems. Therefore, our study showed that the Nigri-nox system works efficiently *in vivo* and could be utilized together with other SSR systems for precisely delineating cell fates *in vivo*.

RESULTS

Generation and characterization of Nigri-nox genetic system

We first generated a new reporter mouse line that responded to Nigri recombinase. By incorporation of the interleaved reporter strategy previously described (He et al., 2017), we arranged one pair of nox sites together with one pair of loxP sites in Rosa26 allele. These two pairs of recombination sites were interleaved in position nox-loxP-nox-loxP such that the recombination of one SSR system removes the recombination site of another SSR system. We knocked CAG-nox-loxP-Stop (transcriptional stop sequence)-nox-ZsGreen-polyA-loxP-tdTomato sequence into the Rosa26 gene locus and named this reporter line as *R*osa26-*n*ox-*l*oxP-*r*eporter, *R26-NLR* (Fig. 1A). For *R26-NLR*, Cre-mediated loxP recombination led to expression of tdTomato reporter, whereas Nigri-mediated nox recombination resulted in expression of ZsGreen reporter (Fig. 1B). The Cre and Nigri recombinases were driven respectively by different cell-specific promoters. For example, cell type A expresses gene A, which drives Nigri; cell type B expresses gene B, which drives Cre, respectively. In the *A-Nigri;B-Cre;R26-NLR* triple positive mouse, we could simultaneously and genetically target two distinct cell populations to understand their cell fates *in vivo* (Fig. 1C).

We next generated *Cdh5-Nigri* by placing Nigri cDNA in-frame with the start codon ATG of the endogenous Cdh5 gene via homologous recombination (Fig. 1D). Correct targeting was verified by long PCR spanning the homology arms. *Cdh5-Nigri* was then crossed with *R26-NLR* to generate *Cdh5-Nigri;R26-NLR* mouse. We collected both embryonic and postnatal mouse tissues for analysis. Whole-mount epi-fluorescence showed ZsGreen^{+} signals in vascular pattern in embryonic day

(E)14.5 embryos and postnatal (P)7 organs (Fig. 1E-F, Fig. S1B). We didn't detect tdTomato$^+$ signal in the tissues, indicating that Nigri recombined nox but not loxP sites. Immunostaining for ZsGreen, tdTomato and endothelial cell maker VE-cadherin (VE-cad) on heart sections showed that almost all endothelial cells (>99%) were ZsGreen$^+$ (Fig. 1G). We didn't detect tdTomato expression in endothelial cells of the heart. Immunostaining for another endothelial cell maker PECAM confirmed that almost all PECAM$^+$ cells were ZsGreen$^+$ (>99%, Fig. 1H). We also performed immunostaining for ZsGreen and tdTomato on serial sections of E15.5 *Cdh5-Nigri;R26-NLR* heart, but didn't find tdTomato$^+$ cell (Fig. S3E). Efficient ZsGreen labeling was also confirmed in other organs or tissues of the *Cdh5-Nigri;R26-NLR* mouse (Fig. S1B,C). To further verify if there was no crosstalk between Nigri-nox and Cre-loxP systems, we performed the following experiments. We isolated endothelial cells of E15.5 *Cdh5-Nigri;R26-NLR* tissues and then performed FACS analysis. We detected that 95.53% ± 1.22% CD31$^+$ endothelial cells were ZsGreen$^+$, but did not detect any tdtomato$^+$ cell by flow cytometry (Fig. S3A). We also performed flow cytometric analysis of E15.5 *Tie2-Cre;R26-GFP* tissues and found that the recombination efficiency of Cre-loxP was 96.40% ± 2.01% (Fig. S3B). There was no significant difference between these two systems (Fig. S3C). Moreover, western blot analysis detected protein expression of ZsGreen but not tdTomato (Fig. S3D). We also crossed *Cdh5-Nigri* with *Rosa26-loxP-Stop-loxP-tdTomato (R26-tdTomato) line* (Madisen et al., 2010) to generate the *Cdh5-Nigri;R26-tdTomato* mouse. We performed immunostaining for tdTomato on heart sections of the *Cdh5-Nigri;R26-tdTomato* mouse but did not detect any tdTomato$^+$ cell (Fig. S1A). Co-transfection assays were also performed to examine the crosstalk *in vitro*. We co-transfected 293T cells with recombinase expression plasmids and recombination reporter plasmids. The pcDNA3.1(-) plasmids were used as controls. We co-transfected pcDNA3.1(-) plasmids with CAG-loxP-STOP-loxP-ZsGreen reporter plasmids or CAG-nox-STOP-nox-ZsGreen reporter plasmids. We then detected very rare leakiness in 4X fields using Olympus microscope. To test if crosstalk between Nigri-nox and Cre-loxP systems existed, we performed co-transfections of pcDNA3.1-Nigri with CAG-loxP-STOP-loxP-ZsGreen reporter plasmids as well as co-transfections of pcDNA3.1-Cre with CAG-nox-STOP-nox-ZsGreen reporter plasmids, respectively. In these experiments, we detected very few ZsGreen$^+$ cell 36 hours post transfection, indicating that the crosstalk between Nigri-nox and Cre-loxP systems was negligible *in vitro*. (Fig. S3F,G). Taken together, these genetic data demonstrated that Nigri specifically and efficiently recombined nox but not loxP sites *in vivo*.

Fate mapping of Cdh5$^+$ endothelial cells by *Cdh5-Nigri*

To further characterize the newly generated *Cdh5-Nigri* mouse line, we collected P7 *Cdh5-Nigri;R26-NLR* mouse heart and examined the cell fate of Cdh5-derived descendants. We stained heart sections with ZsGreen and other cell lineage markers, including fibroblast marker PDGFRa, cardiomyocyte marker Troponin I (TNNI3),

smooth muscle cell marker aSMA and pericyte marker PDGFRb. Consistent with previous reports (de Lange et al., 2004; Lincoln et al., 2004), endothelial cells labeled by *Cdh5-Nigri* contributed to the majority of PDGFRa^{+} mesenchymal cells / fibroblasts in the cardiac valve (Fig. 2A). We did not observe any contribution of endothelial cells to cardiomyocytes (Fig. 2B). Interestingly, a subset of Cdh5-derived cells also expressed aSMA or PDGFRb, indicating that endothelial cells might differentiate into smooth muscle cells or pericytes in the myocardium of developing heart (Fig. 2C-D). This finding is consistent with previous report demonstrating that endothelial cells are progenitors of coronary smooth muscle cells and pericytes (Chen et al., 2016).

Cre recombinase recombines loxP but not nox sites

We next tested whether Cre recombinase recombines nox sites. We used constitutive Cre driven by ACTB promoter that is broadly active in tissues (*ACTB-Cre*) and crossed it with *R26-NLR* mouse line to generate *ACTB-Cre;R26-NLR* (Fig. 3A). Whole-mount epifluorescence of E14.5 *ACTB-Cre;R26-NLR* mouse showed tdTomato^{+} but not ZsGreen^{+} signal, while no tdTomato^{+} cell was detected in the absence of *ACTB-Cre* (Fig. 3B). Immunostaining for tdTomato and ZsGreen on the entire embryonic section and heart section showed tdTomato^{+}ZsGreen^{-} cells (Fig. 3C,D). The same results were obtained at E12.5 and P7 *ACTB-Cre;R26-NLR* tissues (Fig. S2A-C). Western blot analysis of *ACTB-Cre;R26-NLR* tissue also detected protein expression of tdTomato but not ZsGreen (Fig. S3D). To further characterize Cre-loxP recombination in *R26-NLR*, we crossed it with an inducible CreER line that was driven by the ubiquitous gene promoter *UBC-CreER* (Fig. 3E). After tamoxifen induction, both whole-mount epifluorescence and sectional immunostaining showed that most cells were tdTomato^{+}ZsGreen^{-} throughout embryos or heart tissues of the *UBC-CreER;R26-NLR* embryos (Fig. 3F-H, Fig. S2D,F). We didn't detect tdTomato^{+} cell that had not received tamoxifen (Fig. 3G,H). These data demonstrated that both constitutive and inducible Cre recombinases efficiently mediated recombination of loxP site but not nox site. Furthermore, to verify if nox sites could been recognized by other available recombinases such as Dre, we crossed *R26-NLR* with *Tie2-Dre* to generate the *Tie2-Dre;R26-NLR* line. Whole-mount epifluorescence views and sectional staining of E14.5 *Tie2-Dre;R26-NLR* embryos showed no ZsGreen or tdTomato expression, demonstrating that Dre cannot recombine nox sites (Fig. S4). By Nigri-nox and Cre-loxP recombination systems, the new dual reporter *R26-NLR* line could be used to genetically trace the cell fates of two distinct cell populations simultaneously *in vivo*.

Dynamic contribution of distinct progenitor cells to atrioventricular valve mesenchyme

Since our new dual reporter system combines two pairs of recombinase-recognition sites for simultaneous tracking of two distinct progenitor cells, we can study the dynamic contribution of different cell lineages during organ development (e.g. their

component ratio and relative location from early embryonic to postnatal stages) within the same mouse. We then reassessed the dynamic cellular contribution during cardiac valve development. The mammalian heart has four sets of cardiac valves, including the atrioventricular valves (inlet valves such as mitral and tricuspid valves) and the outflow tract valves (outlet valves such as pulmonic and aortic valves) (de Vlaming et al., 2012). During valve formation and morphogenesis, the mesenchymal cells of valves have multiple developmental origins (Snarr et al., 2008; de Vlaming et al., 2012; von Gise and Pu, 2012) (MacGrogan et al., 2014). Previous studies demonstrated that the mesenchymal cells of inlet valves are primarily derived from endocardium (de Lange et al., 2004; Timmerman et al., 2004) (Lincoln et al., 2004; Rivera-Feliciano et al., 2006) and epicardium (Gittenberger-de Groot et al., 1998; Zhou et al., 2010; Wessels et al., 2012), while neural crest and endocardium mainly give rise to outlet valves (Jiang et al., 2000; de Lange et al., 2004; Nakamura et al., 2006). The relative localization and dynamic change of mesenchymal components and ratios of different cell origins remain incompletely understood. We first examined the inlet valve morphogenesis using Nigri-nox and Cre-loxP systems. To trace the fate of epicardial-derived cells and endothelial-derived cells simultaneously, we crossed the *R26-NLR* mouse line with *Tbx18-Cre* (Cai et al., 2008) and *Cdh5-Nigri* mouse line to generate the *Tbx18-Cre;Cdh5-Nigri;R26-NLR* triple positive mouse (Fig. 4A). *Tbx18-Cre* marks the epicardium and is also expressed in few cardiomyocytes (Christoffels et al., 2009), and this study focused on the contribution of epicardial cells to mesenchymal cells in the valve. *Cdh5-Nigri* labeled endocardial cells as ZsGreen and *Tbx18-Cre* labeled epicardial cells as tdTomato (Fig. 4A, Fig. S5A). In order to monitor the dynamic changes of descendants of these two progenitor populations in inlet valve development, we collected hearts for analysis from E12.5 to postnatal day 7 (Fig. 4B). Whole-heart sectional fluorescence of E12.5 *Tbx18-Cre;Cdh5-Nigri;R26-NLR* embryos showed expression of both tdTomato and ZsGreen in the same heart (Fig. 4C). $tdTomato^{+}$ cells were mainly detected in epicardial cells, while $ZsGreen^{+}$ cells were restricted in endocardial cushion as well as endothelial cells at E12.5 (Fig. 4C). At E12.5 and afterwards, epicardial cells form epicardial-derived mesenchymal cells (EPDCs) and differentiate into mesenchymal cells via epithelial-to-mesenchymal transition, EpiMT (Wessels and Perez-Pomares, 2004; Kolditz et al., 2008) (Zhou et al., 2008; Combs and Yutzey, 2009). *Tbx18-Cre* labeled epicardial cells gradually appeared in the partietal but not septal leaflet of tricuspid valve at E14.5 that constituted the majority of mesenchyme at E17.5 and replaced endocardium-derived mesenchyme at P7 (Fig. 4C,D), indicating that EPDCs migrated into the valve and contributed significantly to valve mesenchyme. We also found that endocardium-derived cells constituted almost all valve mesenchyme in the mural leaflet of mitral valve at E12.5 with less contribution from EDPCs (Fig. 4E). At E14.5, EDPCs started to migrate into the proximal mural leaflet and more EDPCs could be found at E17.5 that gradually

constituted the majority of mesenchymal cells in the mural leaflet but not aortic leaflet of the mitral valves by P7 (Fig. 4E,F). The majority of mesenchymal cells in the septal leaflet of tricuspid valve and aortic leaflet of mitral valve were still derived from endocardium (Fig. 4C-F). Quantification of the percentage of ZsGreen^{+} or tdTomato^{+} mesenchymal cells in labeled valve mesenchyme validated the gradual replacement of endocardium-derived cells by EPDCs in partietal leaflet of the tricuspid valve and the mural leaflet of the mitral valve (Fig. 4G).

Dynamic contribution of distinct progenitor cells to outflow track valve mesenchyme

We next used Nigri-nox and Cre-loxP systems to simultaneously monitor contribution of two distinct progenitors in outflow track cushion morphogenesis, remodeling and subsequent semilunar valves formation. Neural crest cells (NCCs) have been reported to contribute primarily to semilunar valves (Jiang et al., 2000; Lincoln et al., 2004; Nakamura et al., 2006). To trace the fate of NCCs and endocardium-derived cells simultaneously, we crossed the *R26-NLR* mouse line with *Wnt1-Cre* and *Cdh5-Nigri* to generate the *Wnt1-Cre;Cdh5-Nigri;R26-NLR* triple positive mouse (Fig. 5A). *Cdh5-Nigri* labeled endocardial cells as ZsGreen and *Wnt1-Cre* labeled neural crest cells as tdTomato (Fig. 5A, Fig. S5B). We analyzed the origins of semilunar valves at embryonic, neonatal, and adult hearts of *Wnt1-Cre;Cdh5-Nigri;R26-NLR* mice (Fig. 5B). At E13.5, NCCs labeled by *Wnt1-Cre* (tdTomato^{+}) contributed to the majority of mesenchymal cells in the right and left posterior cusp of pulmonary valves (PV) adjacent to the aorticopulmonary septum; while endocardial cells labeled by *Cdh5-Nigri* (ZsGreen^{+}) contributed to a substantial number of the distal anterior leaflet of PV (Fig. 5C). For the aortic valves (AoV), tdTomato^{+} NCCs contributed to the majority of mesenchymal cells while ZsGreen^{+} endocardial cells contributed fewer (Fig. 5D). Unlike the atrioventricular valves, endocardial cells constituted the minority of mesenchymal cells in the outflow track valves but they increased gradually from 21.78% ± 4.40% in the embryonic stage to 35.87% ± 1.99% in the adult stage of aortic valves; and from 20.64% ± 1.85% in the embryonic stage to 27.05% ± 5.15% in the adult stage of pulmonary valves during maturation, respectively (Fig. 5E,F). There was a significant difference in the percentage of ZsGreen^{+} mesenchymal cells between E13.5 and 6 week adult valves (Fig. 5E). Taken together, we provide examples to illustrate how Nigri-nox and Cre-loxP systems could be used simultaneously to lineage trace distinct cell populations during development *in vivo*. The dual recombination systems could also be used for studying cell fates of two distinct cell populations during tissue homeostasis and diseases.

DISCUSSION

In this study, we developed a new recombination system (Nigri-nox) for *in vivo* genetic lineage tracing. Nigri-nox recombination is efficient and specific for genomic engineering and does not operate through Cre-loxP (Karimova et al., 2016). Combination of dual recombinases using Nigri and Cre with new dual reporter lines allows genetic lineage tracing of two distinct cell populations. Our work provides proof-of-principle experiments showing that the Nigri-nox system could be used to trace cell fate *in vivo*. Coupled with other recombinases, our results showed genetic targeting of multiple cell lineages in the same mouse.

To prove that this new genetic tool enables genetic tracing of two distinct progenitor populations simultaneously *in vivo*, we used both Nigri-nox and Cre-loxP to reassess the cellular contribution to mesenchyme of cardiac valve during heart development. The inlet atrioventricular valves are primarily derived from endothelium (de Lange et al., 2004; Lincoln et al., 2004) and epicardium (Gittenberger-de Groot et al., 1998; Wessels et al., 2012), whereas the outlet semilunar valves are mainly derived from neural crest and endothelium (Jiang et al., 2000; Nakamura et al., 2006). We generated the triple positive *Tbx18-Cre;Cdh5-Nigri;R26-NLR* mouse line to trace epicardial and endothelial cells simultaneously. We found that these two populations contributed to almost all mesenchymal cells in the inlet valves during valve remodeling. In early embryonic stage, endocardial cells contributed to the majority of mesenchymal cells in both atrioventricular cushions. Whereas from mid-embryonic stage to neonatal stage, the resident endocardium-derived cells of lateral AV cushions were gradually replaced by infiltrating *Tbx18-Cre* labeled EPDCs from proximal to distal. However, endocardium-derived cells still constituted the majority of mesenchyme in septal leaflet of the tricuspid valves and mural leaflet of the mitral valves. We reasoned that this differential component of two leaflets in tricuspid and mitral valves could be due to their distinct anatomic locations in the developing heart. The partietal leaflet of tricuspid is attached to the right ventricular wall and the mural leaflet of the mitral valve is attached to the left ventricular wall, where EPDCs were mostly distributed. Moreover, for analyzing outlet semilunar valves, we also generated triple positive *Wnt1-Cre;Cdh5-Nigri;R26-NLR* line to trace neural crest cells and endothelial cells simultaneously. During valve remodeling from the embryonic to adult stage, contribution of endothelial cells increased gradually in the aortic and pulmonary valves (Fig. 5F). This result might indicate that endocardium-derived mesenchymal cells probably expanded more than neural crest cells during development. Alternatively, endocardium-derived mesenchymal cells could be less sensitive to signals driving apoptosis or valve remodeling.

The dual reporter system *R26-NLR* has advantages in revealing two distinct cell populations. However, this strategy cannot clearly distinguish two cell populations simultaneously if their two promoters are commonly active in an intersection part. If a

lineage-traced cell exhibits activity of both driving promoters at the same time in development, we could label two cell populations by other previously reported intersectional reporters such as *R26::FLAP* (Awatramani et al., 2003), *RC::Fela* (Jensen et al., 2008), *R26NZG* (Yamamoto et al., 2009), *RC::FrePe* (Engleka et al., 2012) and *RC::RLTG* (Plummer et al., 2015). In these alleles, expression of the first reporter located nearby the promoter is controlled by one type of recombinase-mediated recombination, while expression of the second one located far from the promoter requires both types of recombinations. For two different progenitor populations that are driven by two distinct gene promoters, reporter of the first recombination cannot be maintained but replaced by the second reporter after the second round of recombination. Although these intersectional dual-recombinase based reporters allow us to label one group of progenitor cells and its subpopulations, they could not label two separate cell populations defined by two exclusively distinct genes. Here, the property of our new interleaved dual-recombinase based reporter bypassed this pitfall, allowing us to target two distinct progenitor populations simultaneously during development and to trace for their cell fates with distinct lineage tracing reporters (Fig. 6). Together, our novel system provides additional resolutions in cellular dynamics during tissue development.

In summary, our work showed that Nigri-nox was efficient in mammalian genomic engineering and could be utilized with other recombinase systems for more precise genetic targeting *in vivo*. Specifically, Nigri-nox and Cre-loxP systems could target two distinct progenitor cell populations for delineating the contributions of endocardium, neural crest and epicardium cells during cardiac valve development and remodeling. This dual recombination system could also be broadly used in studying various cell lineages in development, diseases and tissue regeneration.

MATERIALS AND METHODS

Mice

All mouse experiments were used in accordance with the guidelines from the Institutional Animal Care and Use Committee (IACUC) of the Institute of Biochemistry and Cell Biology, and Institute for Nutritional Sciences, Shanghai Institutes for Biological Sciences, Chinese Academy of Sciences. *ACTB-Cre, UBC-CreER.* (Liu et al., 2016; Ruzankina et al., 2007) and *Tie2-Cre* mice were described previously (Kisanuki et al., 2001). *Tie2-Dre* mouse was reported previously by our lab (Pu et al., 2018). *R26-NLR* mouse line was generated by knocking CAG-nox-loxP-Stop-nox-ZsGreen-polyA-loxP-wpre-Frt-Neo-Frt into intron 1 of Rose26 locus through homologous recombination. *Cdh5-Nigri* knock-in mouse line was generated by homologous recombination using CRISPR/Cas9 methods. For *Cdh5-Nigri* line, a cDNA encoding Nigri cassette was inserted into the second exon of Cdh5 gene. *Cdh5-Nigri* line result in heterozygosity of Cdh5 gene. *Cdh5-Nigri* and *R26-NLR* knock-in lines were generated by Shanghai Biomodel Organism Science

and Technology Development Co., Ltd,. Shanghai, China. All mice used in this study were maintained on a C57BL6/ICR background. Tamoxifen (Sigma, T5648-5G) was dissolved in corn oil and administrated to mice by oral gavage at indicated time (0.2 mg/g).

Genomic PCR

Genomic DNA was extracted from mouse tail. Tissues were lysed in lysis buffer (100 μg/ml proteinase K) overnight at 55°C and the mixture was centrifuged at the maximum speed for 8 min to obtain supernatant with genomic DNA the next day. DNA was precipitated by isopropanol, and then washed in 70% ethanol by centrifugation for 3 min. Finally, DNA was dissolved in deionized water. All the mice or embryos were genotyped using genomic PCR to distinguish knock-in allele from wild-type allele. For the *R26-NLR* line, Primers 5'-TCCCGACAAAACCGAAAATCTGTGG-3' and 5'-TGCATCGCATTGTCTGAGTAGG-3' were used to detect the *R26-NLR* positive allele, and 5'-TCCCGACAAAACCGAAAATCTGTGG-3' and 5'-GGGGCGTGCTGAGCCAGACCTCCAT-3' were used to detect the wild-type allele. For the *Cdh5-Nigri* line, primers 5'-GGAGCCAGGCGCATAGTGAGCA-3' and 5'-GGTAGGGGCGGTGGTTCTGGTG-3' were used to detect the Nigri positive allele, and 5'-TTTCCCCAGATCAGCTCCTCCAC-3' and 5'-CCCCCGCACCACCAATGATA-3' were used to detect the wild-type allele.

Tissue collection and Immunostaining

Immunostaining in this study was performed as previously described (Zhang et al., 2016). Briefly, mouse embryos or hearts were collected in PBS on ice and then washed gently to remove blood. They were then fixed in 4% PFA for 15-60 min at 4°C depending on tissue size. After washing several times in PBS, we could use fluorescence microscopy (Zeiss AXIO Zoom V16) to take photographs of embryos or hearts with indicated fluorescence reporters. After that, the embryos or hearts were dehydrated in 30% sucrose/PBS for several hours or overnight at 4°C, and then embedded in OCT (Sakura) the next day. Frozen sections of 7-10 μm were collected on slides. For immunostaining, tissue sections were first washed in PBS to remove OCT, and then blocked in 5% PBSST (5% donkey serum/0.1% Triton X-100/PBS) for 30 min at room temperature and then incubated with primary antibodies overnight at 4°C. Primary antibodies against the following proteins and dilution were used: tdTomato (Rockland, 600-401-379; 1:1,000 dilution), ZsGreen (Clontech, 632474; 1:1000), VE-cad (R&D, AF1002; 1:100 dilution), PECAM (BD, 553370; 1:500), PDGFRa (eBioscience, 14-1401-81; 1:500), PDGFRa (R&D, AF1062; 1:500), PDGFRb (eBioscience, 14-1402; 1:500), aSMA (Sigma, F3777; 1:500), TNNI3 (Abcam, ab56357; 1:200). In the next day, sections were washed with PBS for several times and then incubated with Alexa fluorescence secondary antibodies and conterstained with DAPI (Vector Laboratories) at room temperature for 40 min in dark. After washed several times in PBS, all slides were mounted with mounting

medium. For weak signals, HRP-conjugated secondary antibodies were used to amplify the signals. Images were acquired by Olympus confocal microscopy system (FV1200), Leica confocal (TCS SP5). To provide Z-stack images, we scanned 5-10 consecutive *xy* images on the *z*-axis using confocal microscope. The images were analyzed by ImageJ (NIH) software.

Western blot

Tissues of *R26-NLR* mice, *ACTB-Cre;R26-NLR* mice and *Cdh5-Nigri;R26-NLR* mice were collected and dissected. Protein supernatant was obtained after homogenized in Tris-SDS lysis buffer (1%SDS, 50 mM Tris-HCl, pH 8.0), incubated at 4°C for 30 min and centrifuged at max speed for 5 min. After mixed 4:1 with 5x loading buffer (10% SDS, 0.3 M Tris=HCl, 1.5 M dithiothreitol, pH 6.8), protein samples were boiled for 10 min, separated by 10% SDS-PAGE and then transferred by a Mini Trans Blot system (Bio-Rad) onto a polyvinylidene fluoride (PVDF) membrane (Immobilon, Millipore). The membrane was blocked with 5% BSA dissolved in TBS-T (150 mM NaCl, 0.5% vol/vol Tween-20, 10 mM Tris-HCl) at room temperature for 1 h and incubated with primary antibody at 4°C overnight. After washed for three times with TBS-T, the membrane was incubated with HRP-conjugated secondary antibody at room temperature for 1 h. Then the membrane was washed with TBS-T three times for 30 min. Proteins bands were observed by enhanced chemiluminescence (Pierce). Antibodies used in this study were as follows: ZsGreen (rabbit, Clontech, 632474; 1:1000), tdTomato (rabbit, Rockland, 600-401-379; 1:1000 dilution), anti-β-actin (mouse, Cell Signaling, 3700; 1:1000), HRP-anti-rabbit IgG (Jackson ImmunoResearch, 711-035-152; 1:4000), HRP-anti-mouse IgG (Jackson ImmunoResearch, 115-035-174; 1:4000).

Flow cytometry

Endothelial cells were isolated from *Cdh5-Nigri;R26-NLR* and *Tie2-Cre;R26-GFP* mice. Briefly, tissues from *Cdh5-Nigri;R26-NLR* and *Tie2-Cre;R26-GFP* mice were dissected and cut into small pieces. They were then digested by lysis buffer that contained DNase I and collagenase type II at 37°C for 40 min. After digestion, this buffer was passed through 70 mm cell strainers. The cells were centrifuged at 1000 g for 5 min at 4°C. Blood cells were lysed by Red Blood Cell lysis buffer (eBioscience, 00-4333-57) and the cells were re-suspended and washed in PBS. After that, 500 µl isolation buffer (0.5% BSA and 2 mM EDTA in PBS) was used to wash the cells, then centrifuged for 2 min at 4600 g. The cells were stained with antibody containing CD45 PE-Cy7 (eBioscience, 25-0451, 1:400), Ter-119 PE-Cy7 (eBioscience, 25-5921, 1:400), or CD31 APC (eBioscience, 17-0311-82, 1:40) for 30 min at 4°C. Finally, the cells were washed in isolation buffer and re-suspended in PBS. FACS Aria II Flow

Cytometer (BD Bioscience) was used to analyze the stained cells. Flowjo (TreeStar) was used to process the raw data with quantification analysis.

Co-transfection assay

We co-transfected 293T cells with recombinase expression plasmids and recombination reporter plasmids to test if there exists crosstalk between Nigri-nox and Cre-loxP systems. Two recombinase expression plasmids (pcDNA3.1-Cre, pcDNA3.1-Nigri) and two recombination reporter plasmids (CAG-loxP-STOP-loxP-ZsGreen, CAG-nox-STOP-nox-ZsGreen) were used in this assay. The pcDNA3.1(-) plasmids were used as controls. The assay was performed using Lipofectamine 3000 Transfection Reagent (Invitrogen). Briefly, 293T cells were plated at the density of 5×10^5 cells per well in 12-well dishes. And the cells were cultured in Dulbecco's Modified Eagle Medium (DMEM) containing 10% fetal bovine serum (Invitrogen), 1% Penicillin-Streptomycin-Glutamine (PSG, Invitrogen). Then we co-transfected 293T cells with plasmids. We designed six groups of experiments and three repeats in each group. Group one and group two were negative control groups and the cells were co-transfected with pcDNA3.1(-) plasmids containing CAG-loxP-STOP-loxP-ZsGreen reporter plasmids or CAG-nox-STOP-nox-ZsGreen reporter plasmids, respectively. Group three and group four were positive control groups. One group was co-transfected with pcDNA3.1-Nigri and CAG-nox-STOP-nox-ZsGreen reporter plasmids and another group was co-transfected with pcDNA3.1-Cre and CAG-loxP-STOP-loxP-ZsGreen reporter plasmids. Group five and group six were used to test if there exists crosstalk between Nigri-nox and Cre-loxP systems. One group was co-transfected with pcDNA3.1-Nigri and CAG-loxP-STOP-loxP-ZsGreen reporter plasmids and cells from another group were co-transfected with pcDNA3.1-Cre and CAG-nox-STOP-nox-ZsGreen reporter plasmids. Then the cells were culture in 5% CO2 at 37°C. The expression of ZsGreen were analyzed 36 hours after transfection using an Olmypus BX53 microscope.

Statistics analysis

All data were obtained from 4-6 independent experiments as indicated in each figure legend. Immunostaining of ZsGreen and tdTomato was used to indicate dual lineage tracing of progenitor-derived cells. ZsGreen indicates endocardial-derived cells (*Cdh5-Nigri*). tdTomato indicates epicardial-derived cells (*Tbx18-Cre*) or neural crest cell-derived cells (*Wnt1-Cre*). The proportion of fluorescent area between ZsGreen and tdTomato in heart valves indicates the ratio of two groups of labeled cells. The signals of ZsGreen removed PECAM was used for statistics because $PECAM^+$ valve endothelial cells were also labeled by ZsGreen. Fluorescence signals were analyzed by ImageJ software. All data were presented as mean values ± SEM. Two-tailed

unpaired Student's *t*-test was used to compare the difference between two groups; ANOVA test was used to compare differences among three or more groups. $P < 0.05$ was accepted as statistically significant.

Acknowledgements

We thank Shanghai Biomodel Organism Co., Ltd. for mouse generation. We also thank Baojin Wu, Guoyuan Chen, Zhonghui Weng and Aimin Huang for the animal husbandry; Wei Bian for technical help and the National Center for Protein Science Shanghai for helping in confocal imaging.

Competing interests

The authors declare no competing or financial interests.

Author contributions

K.L. and B.Z. designed the study, performed experiments and analyzed the data. W.Y., M.T., J.T., X.L., Q.L., Y.L., L.H., X.T., L.Z. bred the mice, performed experiments and provided valuable comments. S.E. provided *Tbx18-Cre* line and provided valuable comments on the work. K.O.L. edited the manuscript, analyzed data and provided suggestions. B.Z. supervised the study, analyzed the data and wrote the manuscript.

Funding

This work was supported by the National key Research & Development Program of China (2016YFC1300600 and 2017YFC1001303, SQ2018YFA010113, SQ2018YF010021), Strategic Priority Research Program of the Chinese Academy of Sciences (CAS, XDB19000000, XDA16020204), National Science Foundation of China (31730112, 91639302, 31625019, 81761138040， 31571503, 31501172, 31601168, 31701292, 91749122), Youth Innovation Promotion Association of CAS (2015218, 2060299), Key Project of Frontier Sciences of CAS (QYZDB-SSW-SMC003), International Cooperation Fund of CAS, Shanghai Science and Technology Commission (17ZR1449600, 17ZR1449800), The Program for Guangdong Introducing Innovative and Enterpreneurial Teams (2017ZT07S347), Shanghai Yangfan Project (16YF1413400, 18YF1427600) and Rising-Star Program (15QA1404300), China Postdoctoral Science Foundation (2016M600337, 2017M611634, 2017M621552, 2016LH0042), China Postdoctoral Innovative Talent Support Program (BX201700267), China Young Talents Lift Engineering (YESS20160050, 2017QNRC001), Astrazeneca, Boehringer Ingelheim, Sanofi-SIBS

Fellowship, Royal Society-Newton Advanced Fellowship (NA170109), Research Council of Hong Kong (04110515, 14111916, C4024-16W) and Health and Medical Research Fund (03140346, 04152566).

Supplementary material

Supplementary figures 1-5.

References

Anastassiadis, K., Fu, J., Patsch, C., Hu, S., Weidlich, S., Duerschke, K., Buchholz, F., Edenhofer, F. and Stewart, A. F. (2009). Dre recombinase, like Cre, is a highly efficient site-specific recombinase in E. coli, mammalian cells and mice. *Dis Model Mech* **2**, 508-515.

Awatramani, R., Soriano, P., Rodriguez, C., Mai, J. J. and Dymecki, S. M. (2003). Cryptic boundaries in roof plate and choroid plexus identified by intersectional gene activation. *Nat Genet* **35**, 70-75.

Buckingham, M. E. and Meilhac, S. M. (2011). Tracing cells for tracking cell lineage and clonal behavior. *Dev Cell* **21**, 394-409.

Cai, C. L., Martin, J. C., Sun, Y., Cui, L., Wang, L., Ouyang, K., Yang, L., Bu, L., Liang, X., Zhang, X. et al. (2008). A myocardial lineage derives from Tbx18 epicardial cells. *Nature* **454**, 104-108.

Chen, Q., Zhang, H., Liu, Y., Adams, S., Eilken, H., Stehling, M., Corada, M., Dejana, E., Zhou, B. and Adams, R. H. (2016). Endothelial cells are progenitors of cardiac pericytes and vascular smooth muscle cells. *Nat Commun* **7**, 12422.

Christoffels, V. M., Grieskamp, T., Norden, J., Mommersteeg, M. T., Rudat, C. and Kispert, A. (2009). Tbx18 and the fate of epicardial progenitors. *Nature* **458**, E8-9; discussion E9-10.

Combs, M. D. and Yutzey, K. E. (2009). Heart valve development: regulatory networks in development and disease. *Circ Res* **105**, 408-421.

de Lange, F. J., Moorman, A. F., Anderson, R. H., Manner, J., Soufan, A. T., de Gier-de Vries, C., Schneider, M. D., Webb, S., van den Hoff, M. J. and Christoffels, V. M. (2004). Lineage and morphogenetic analysis of the cardiac valves. *Circ Res* **95**, 645-654.

Devine, W. P., Wythe, J. D., George, M., Koshiba-Takeuchi, K. and Bruneau, B. G. (2014). Early patterning and specification of cardiac progenitors in gastrulating mesoderm. *eLife* **3**.

de Vlaming, A., Sauls, K., Hajdu, Z., Visconti, R. P., Mehesz, A. N., Levine, R. A., Slaugenhaupt, S. A., Hagège, A., Chester, A. H., Markwald, R. R. et al. (2012). Atrioventricular valve development: new perspectives on an old theme. *Differentiation* **84**, 103-116.

Engleka, K. A., Manderfield, L. J., Brust, R. D., Li, L., Cohen, A., Dymecki, S. M. and Epstein, J. A. (2012). Islet1 derivatives in the heart are of both neural crest and second heart field origin. *Circ Res* **110**, 922-926.

Fenno, L. E., Mattis, J., Ramakrishnan, C., Hyun, M., Lee, S. Y., He, M.,

Tucciarone, J., Selimbeyoglu, A., Berndt, A., Grosenick, L. et al. (2014). Targeting cells with single vectors using multiple-feature Boolean logic. *Nat Methods* **11**, 763-772.

Gittenberger-de Groot, A. C., Vrancken Peeters, M. P., Mentink, M. M., Gourdie, R. G. and Poelmann, R. E. (1998). Epicardium-derived cells contribute a novel population to the myocardial wall and the atrioventricular cushions. *Circ Res* **82**, 1043-1052.

He, L., Li, Y., Li, Y., Pu, W., Huang, X., Tian, X., Wang, Y., Zhang, H., Liu, Q., Zhang, L. et al. (2017). Enhancing the precision of genetic lineage tracing using dual recombinases. *Nat Med* **23**, 1488-1498.

Jensen, P., Farago, A. F., Awatramani, R. B., Scott, M. M., Deneris, E. S. and Dymecki, S. M. (2008). Redefining the serotonergic system by genetic lineage. *Nat Neurosci* **11**, 417-419.

Jiang, X., Rowitch, D. H., Soriano, P., McMahon, A. P. and Sucov, H. M. (2000). Fate of the mammalian cardiac neural crest. *Development* **127**, 1607-1616.

Karimova, M., Splith, V., Karpinski, J., Pisabarro, M. T. and Buchholz, F. (2016). Discovery of Nigri/nox and Panto/pox site-specific recombinase systems facilitates advanced genome engineering. *Sci Rep* **6**, 30130.

Kisanuki, Y. Y., Hammer, R. E., Miyazaki, J., Williams, S. C., Richardson, J. A. and Yanagisawa, M. (2001). Tie2-Cre transgenic mice: a new model for endothelial cell-lineage analysis in vivo. *Dev Biol* **230**, 230-242.

Kolditz, D. P., Wijffels, M. C., Blom, N. A., van der Laarse, A., Hahurij, N. D., Lie-Venema, H., Markwald, R. R., Poelmann, R. E., Schalij, M. J. and Gittenberger-de Groot, A. C. (2008). Epicardium-derived cells in development of annulus fibrosis and persistence of accessory pathways. *Circulation* **117**, 1508-1517.

Kretzschmar, K. and Watt, F. M. (2012). Lineage tracing. *Cell* **148**, 33-45.

Lincoln, J., Alfieri, C. M. and Yutzey, K. E. (2004). Development of heart valve leaflets and supporting apparatus in chicken and mouse embryos. *Dev Dyn* **230**, 239-250.

Liu, Q., Yang, R., Huang, X., Zhang, H., He, L., Zhang, L., Tian, X., Nie, Y., Hu, S., Yan, Y. et al. (2016). Genetic lineage tracing identifies in situ Kit-expressing cardiomyocytes. *Cell Res* **26**, 119-130.

Livet, J., Weissman, T. A., Kang, H., Draft, R. W., Lu, J., Bennis, R. A., Sanes, J. R. and Lichtman, J. W. (2007). Transgenic strategies for combinatorial expression of fluorescent proteins in the nervous system. *Nature* **450**, 56-62.

MacGrogan, D., Luxán, G., Driessen-Mol, A., Bouten, C., Baaijens, F. and de la Pompa, J. L. (2014). How to make a heart valve: from embryonic development

to bioengineering of living valve substitutes. *Cold Spring Harb Perspect Med* **4**, a013912.

Madisen, L., Zwingman, T. A., Sunkin, S. M., Oh, S. W., Zariwala, H. A., Gu, H., Ng, L. L., Palmiter, R. D., Hawrylycz, M. J., Jones, A. R. et al. (2010). A robust and high-throughput Cre reporting and characterization system for the whole mouse brain. *Nat Neurosci* **13**, 133-140.

Nakamura, T., Colbert, M. C. and Robbins, J. (2006). Neural crest cells retain multipotential characteristics in the developing valves and label the cardiac conduction system. *Circ Res* **98**, 1547-1554.

Plummer, N. W., Evsyukova, I. Y., Robertson, S. D., de Marchena, J., Tucker, C. J. and Jensen, P. (2015). Expanding the power of recombinase-based labeling to uncover cellular diversity. *Development* **142**, 4385-4393.

Pu, W., He, L., Han, X., Tian, X., Li, Y., Zhang, H., Liu, Q., Huang, X., Zhang, L., Wang, Q. D., et al. (2018). Genetic Targeting of Organ-Specific Blood Vessels. *Circ Res* **123**, 86-99.

Rivera-Feliciano, J., Lee, K. H., Kong, S. W., Rajagopal, S., Ma, Q., Springer, Z., Izumo, S., Tabin, C. J. and Pu, W. T. (2006). Development of heart valves requires Gata4 expression in endothelial-derived cells. *Development* **133**, 3607-3618.

Rodriguez, C. I., Buchholz, F., Galloway, J., Sequerra, R., Kasper, J., Ayala, R., Stewart, A. F. and Dymecki, S. M. (2000). High-efficiency deleter mice show that FLPe is an alternative to Cre-loxP. *Nat Genet* **25**, 139-140.

Ruzankina, Y., Pinzon-Guzman, C., Asare, A., Ong, T., Pontano, L., Cotsarelis, G., Zediak, V. P., Velez, M., Bhandoola, A. and Brown, E. J. (2007). Deletion of the developmentally essential gene ATR in adult mice leads to age-related phenotypes and stem cell loss. *Cell Stem Cell* **1**, 113-126.

Sauer, B. and Henderson, N. (1988). Site-specific DNA recombination in mammalian cells by the Cre recombinase of bacteriophage P1. *Proc Natl Acad Sci U S A* **85**, 5166-5170.

Schonhuber, N., Seidler, B., Schuck, K., Veltkamp, C., Schachtler, C., Zukowska, M., Eser, S., Feyerabend, T. B., Paul, M. C., Eser, P. et al. (2014). A next-generation dual-recombinase system for time- and host-specific targeting of pancreatic cancer. *Nat Med*

Snarr, B. S., Kern, C. B. and Wessels, A. (2008). Origin and fate of cardiac mesenchyme. *Dev Dyn* **237**, 2804-2819.

Snippert, H. J., van der Flier, L. G., Sato, T., van Es, J. H., van den Born, M., Kroon-Veenboer, C., Barker, N., Klein, A. M., van Rheenen, J., Simons, B. D. et al. (2010). Intestinal crypt homeostasis results from neutral competition

between symmetrically dividing Lgr5 stem cells. *Cell* **143**, 134-144.

Soriano, P. (1999). Generalized lacZ expression with the ROSA26 Cre reporter strain. *Nat Genet* **21**, 70-71.

Srinivas, S., Watanabe, T., Lin, C. S., William, C. M., Tanabe, Y., Jessell, T. M. and Costantini, F. (2001). Cre reporter strains produced by targeted insertion of EYFP and ECFP into the ROSA26 locus. *BMC Dev Biol* **1**, 4.

Timmerman, L. A., Grego-Bessa, J., Raya, A., Bertran, E., Perez-Pomares, J. M., Diez, J., Aranda, S., Palomo, S., McCormick, F., Izpisua-Belmonte, J. C. et al. (2004). Notch promotes epithelial-mesenchymal transition during cardiac development and oncogenic transformation. *Genes Dev* **18**, 99-115.

von Gise, A. and Pu, W. T. (2012). Endocardial and epicardial epithelial to mesenchymal transitions in heart development and disease. *Circ Res* **110**, 1628-1645.

Wessels, A. and Perez-Pomares, J. M. (2004). The epicardium and epicardially derived cells (EPDCs) as cardiac stem cells. *Anat Rec A Discov Mol Cell Evol Biol* **276**, 43-57.

Wessels, A., van den Hoff, M. J., Adamo, R. F., Phelps, A. L., Lockhart, M. M., Sauls, K., Briggs, L. E., Norris, R. A., van Wijk, B., Perez-Pomares, J. M. et al. (2012). Epicardially derived fibroblasts preferentially contribute to the parietal leaflets of the atrioventricular valves in the murine heart. *Dev Biol* **366**, 111-124.

Yamamoto, M., Shook, N. A., Kanisicak, O., Yamamoto, S., Wosczyna, M. N., Camp, J. R. and Goldhamer, D. J. (2009). A multifunctional reporter mouse line for Cre- and FLP-dependent lineage analysis. *Genesis* **8**, 53-54.

Zhang, H., Pu, W., Liu, Q., He, L., Huang, X., Tian, X., Zhang, L., Nie, Y., Hu, S., Lui, K. O. et al. (2016). Endocardium Contributes to Cardiac Fat. *Circ Res* **118**, 254-265.

Zhou, B., Ma, Q., Rajagopal, S., Wu, S. M., Domian, I., Rivera-Feliciano, J., Jiang, D., von Gise, A., Ikeda, S., Chien, K. R. et al. (2008). Epicardial progenitors contribute to the cardiomyocyte lineage in the developing heart. *Nature* **454**, 109-113.

Zhou, B., von Gise, A., Ma, Q., Hu, Y. W. and Pu, W. T. (2010). Genetic fate mapping demonstrates contribution of epicardium-derived cells to the annulus fibrosis of the mammalian heart. *Dev Biol* **338**, 251-261.

Figures

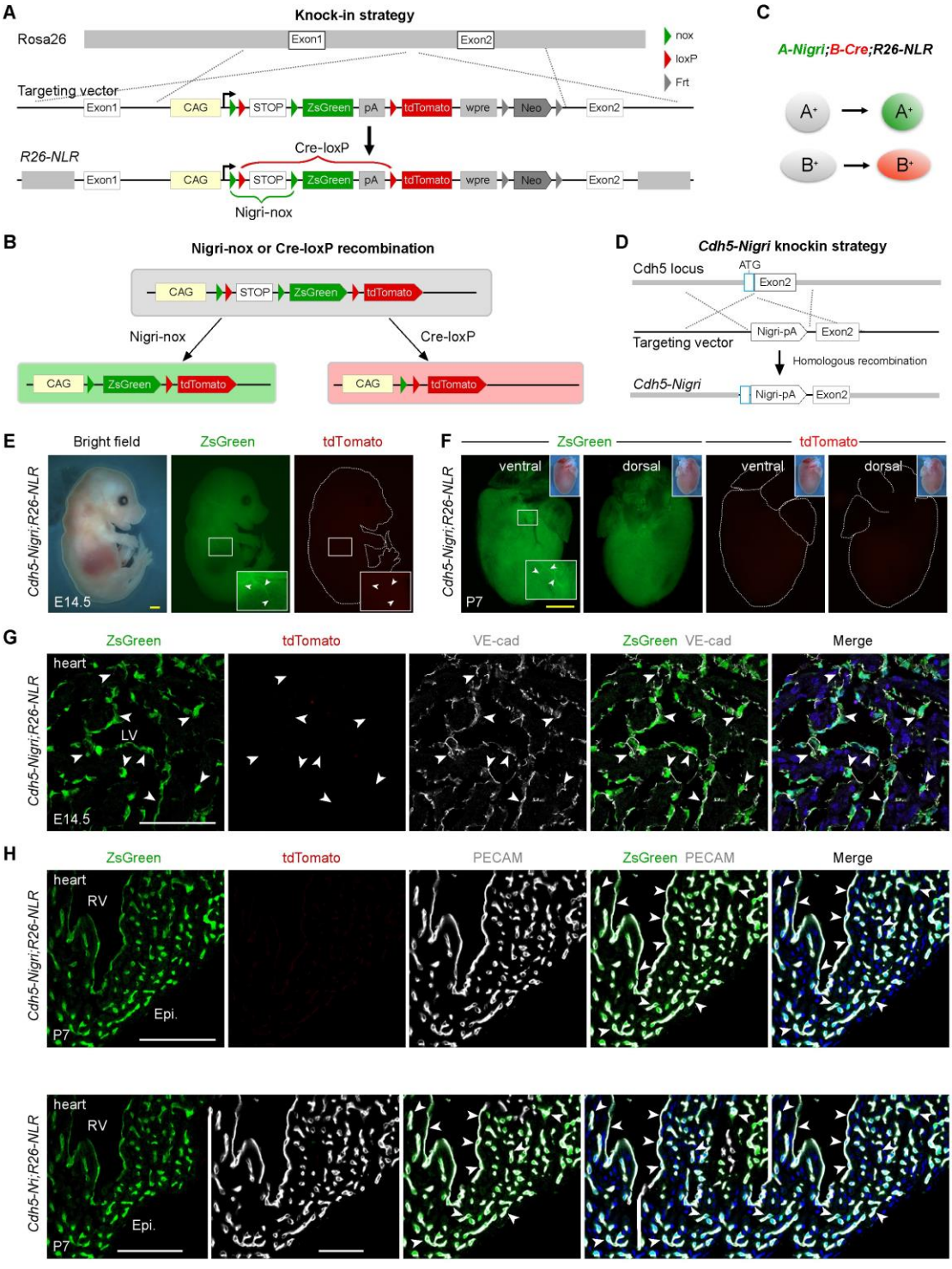

Fig. 1. Generation and characterization of *R26-NLR* and *Cdh5-Nigri* mouse lines. (A) Schematic diagram showing knock-in strategy of dual reporter line *R26-NLR* by homologous recombination. (B,C) Schematic figure showing the recombination result by crossing *R26-NLR* with *A-Nigri* and *B-Cre* mice lines. (D) Knock-in strategy for generation of *Cdh5-Nigri* mouse by homologous recombination. (E,F) Wholemount views of E14.5 *Cdh5-Nigri;R26-NLR* embryo (E) and P7 *Cdh5-Nigri;R26-NLR* heart (F). The insets are magnified images of the boxed regions. Arrowheads indicate ZsGreen^{+} vessels. (G) Immunostaining for ZsGreen, tdTomato and VE-cad on E14.5 *Cdh5-Nigri;R26-NLR* embryonic section shows VE-cad^{+} endothelial cells are ZsGreen^{+} (arrowheads). (H) Immunostaining for ZsGreen, tdTomato and PECAM on P7 *Cdh5-Nigri;R26-NLR* heart section shows efficient labeling of endothelial cells by ZsGreen (arrowheads). LV, left ventricle. RV, right ventricle. Epi, Epicardium. Yellow bar, 1 mm; white bar, 100 μm. Each image is representative of 4-5 individual biological samples.

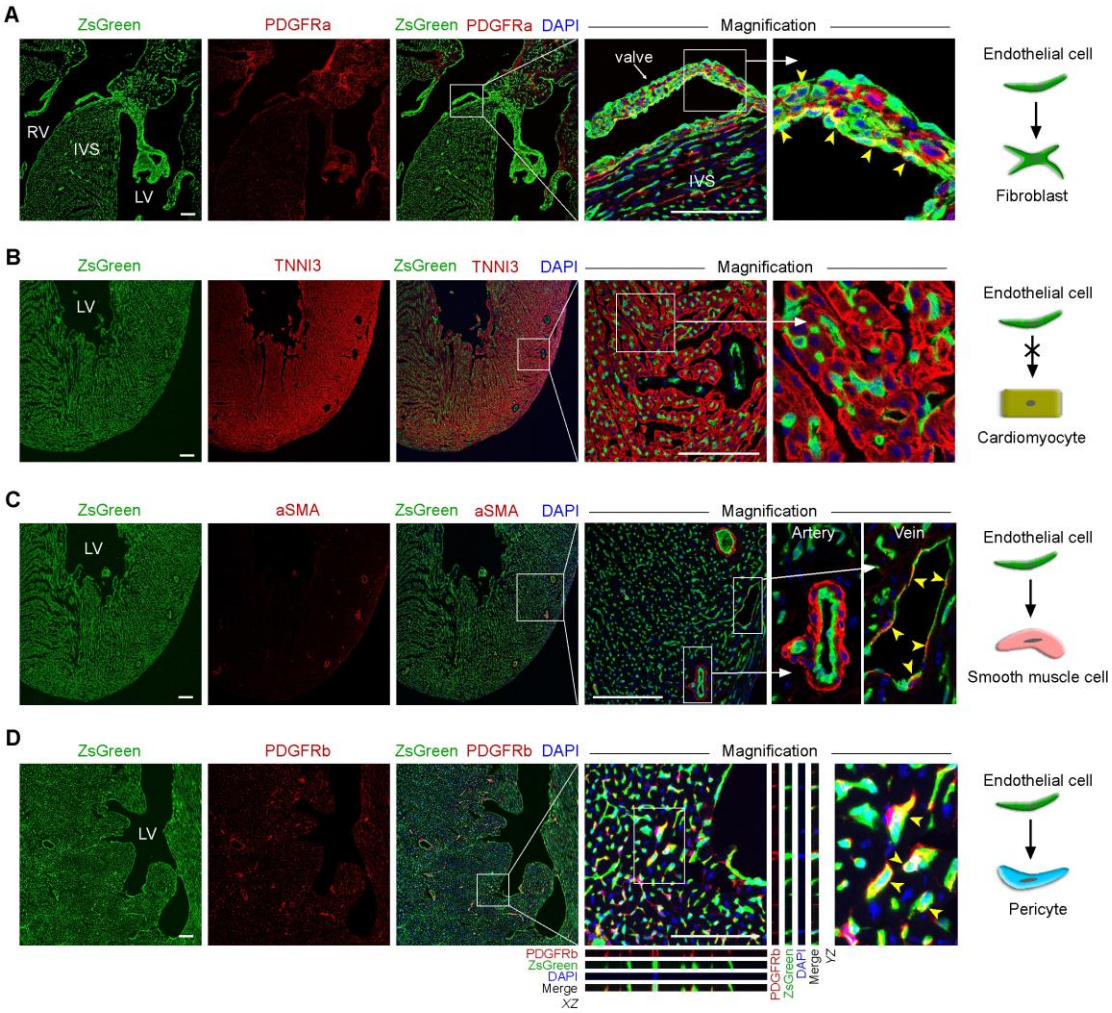

Fig. 2. Cardiac cell lineages labeled by *Cdh5-Nigri*. (A) Immunostaining for ZsGreen and PDGFRa on heart sections shows that *Cdh5-Nigri* labeled endothelial cells give rise to the fibroblasts of valve. Boxed regions are magnified in the right panels. (B) Immunostaining for ZsGreen and TNNI3 on heart sections shows that *Cdh5-Nigri* labeled cells do not contribute to cardiomyocytes. (C) Immunostaining for ZsGreen and aSMA on heart sections shows that *Cdh5-Nigri* labeled cells contribute to a subset of smooth muscle cells. Yellow arrowheads indicate ZsGreen^{+}aSMA^{+} smooth muscle cells. (D) Immunostaining for ZsGreen and PDGFRb on heart sections shows that *Cdh5-Nigri* labeled cells give rise to a subset of pericytes during heart development. Right channels are Z-stack confocal images. RA, right atrium. RV, right ventricle. LV, right ventricle. IVS, interventricular septum. Scale bars, 100 μm.

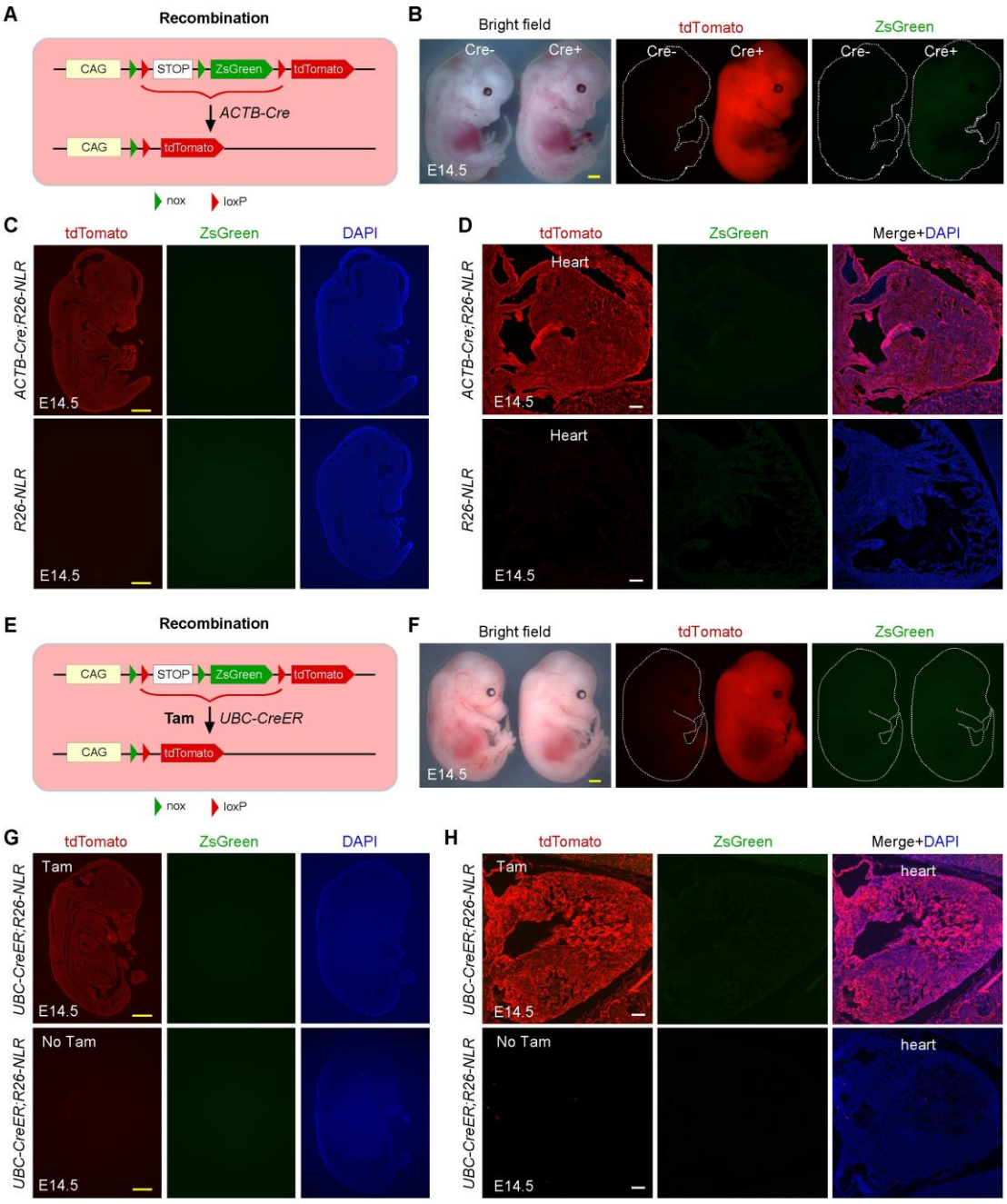

Fig. 3. Cre recombinase recombines loxP but not nox sites in *R26-NLR* line. (A) Schematic figure showing crossing of *ACTB-Cre* with dual reporter line *R26-NLR*, and Cre-loxP recombination. (B) Wholemount bright-field and epifluorescence views of E14.5 *ACTB-Cre;R26-NLR* embryo. Cre- indicates the control embryo with genotype of *R26-NLR* and Cre+ indicates the mutant embryo with genotype of *ACTB-Cre;R26-NLR*. (C) Immunostaining for ZsGreen and tdTomato on E14.5 Cre+ and Cre- embryos. (D) Magnification views of heart in (C) show all cells are $tdTomato^{+}$ $ZsGreen^{-}$ in Cre+ embryo and

no fluorescent cells in Cre- embryo. (E,F) Schematic figure showing crossing of inducible *UBC-CreER* with dual reporter line *R26-NLR* and CreER-loxP recombination after Tamoxifen (Tam) treatment at E12.5. (G) Wholemount bright-field and fluorescence views of E14.5 *UBC-CreER;R26-NLR* embryo. (G,H) Immunostaining for ZsGreen and tdTomato on E14.5 *UBC-CreER;R26-NLR* embryo show all cells are $tdTomato^{+}$ $ZsGreen^{-}$ after Tam induction. Yellow bar, 1 mm; white bar, 100 μm. Each image is representative of 4-5 individual biological samples.

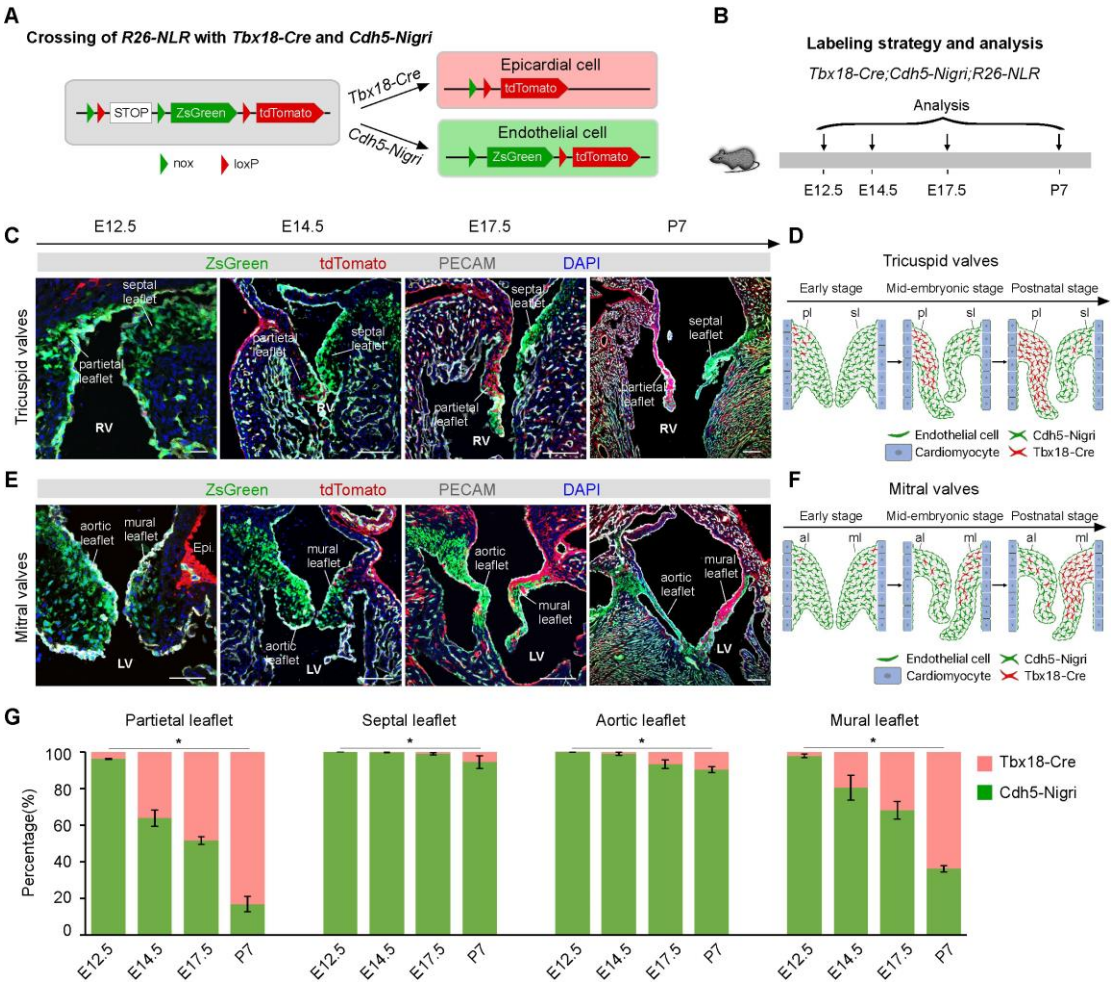

Fig. 4. Simultaneous tracing of two genetically distinct progenitor cell populations for atrioventricular valve mesenchyme. (A) Schematic diagram showing recombinations of *R26-NLR* with *Tbx18-Cre* and *Cdh5-Nigri*. (B) Schematic figure showing time points for tissue analysis. (C) Immunostaining for ZsGreen, tdTomato and PECAM on heart sections. (D) Cartoon showing the contribution of *Tbx18-Cre* and *Cdh5-Nigri* to tricuspid valves development. (E) Immunostaining for ZsGreen, tdTomato, and PECAM on heart sections. (F) Cartoon showing the contribution of *Tbx18-Cre* and *Cdh5-Nigri* to mitral valves development. (G) Quantification the percentage of mesenchymal cells labeled by *Tbx18-Cre* and *Cdh5-Nigri* during atrioventricular valves development. **P* < 0.05; LV, left ventricle. RV, right ventricle. pl, partietal leaflet. sl, septal leaflet. al, aortic leaflet. ml, mural leaflet. Epi, Epicardium. Scale bar, 100 μm. Each image is representative of 4-5 individual biological samples.

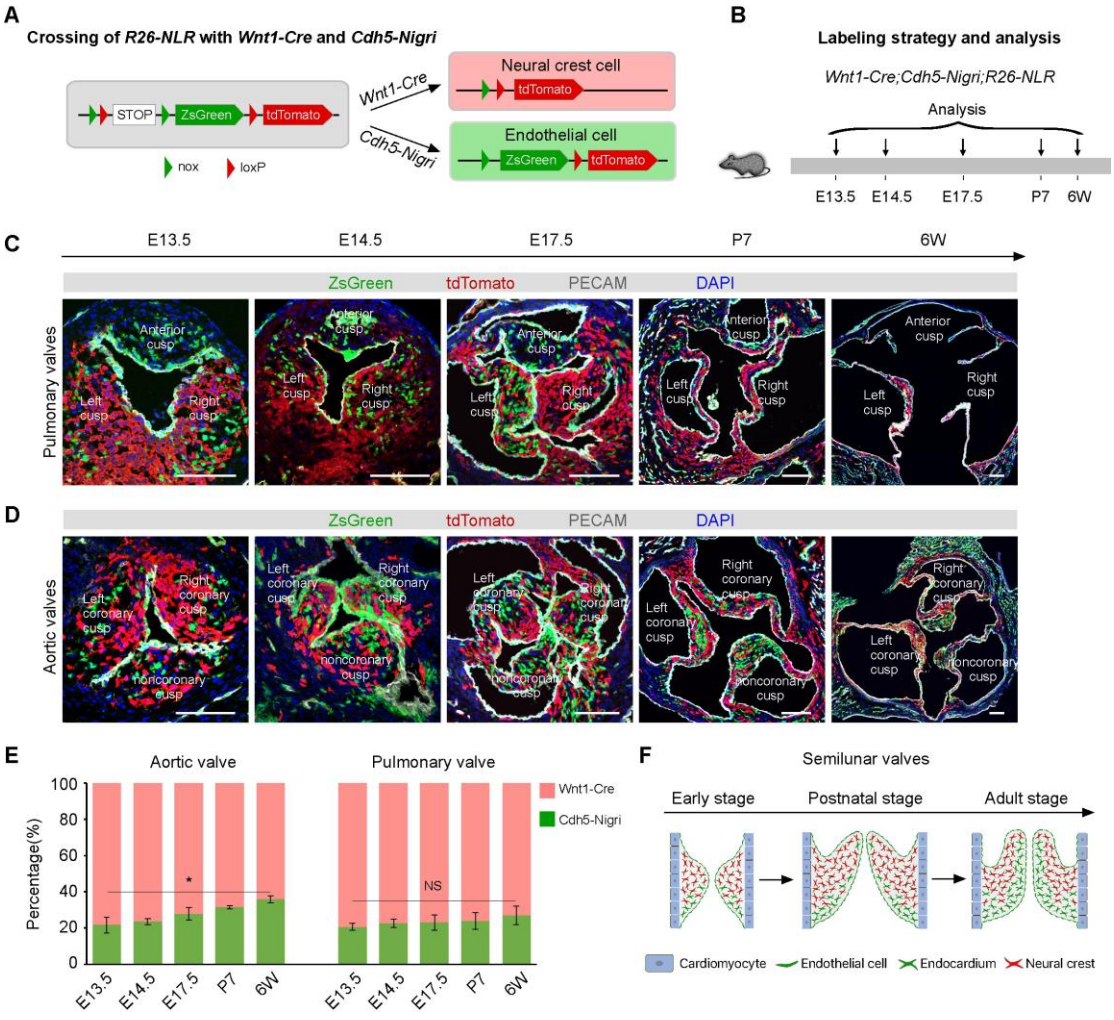

Fig. 5. Simultaneous tracing of two genetically distinct progenitor cell populations for outflow tract valve mesenchyme. (A) Schematic diagram showing recombinations of *R26-NLR* with *Wnt1-Cre* and *Cdh5-Nigri*. (B) Schematic figure showing time points of tissue analysis. (C) Immunostaining for ZsGreen, tdTomato and PECAM on heart sections containing pulmonary valves. (D) Immunostaining for ZsGreen, tdTomato, and PECAM on heart sections containing aortic valves. (E) Quantification the percentage of cells labeled by *Wnt1-Cre* and *Cdh5-Nigri* during semilunar valves development. **P* < 0.05; NS, non-significant. (F) Cartoon showing the contribution of endocardium and neural crest to semilunar valves development. Scale bar, 100 μm. Each image is representative of 4-5 individual biological samples.

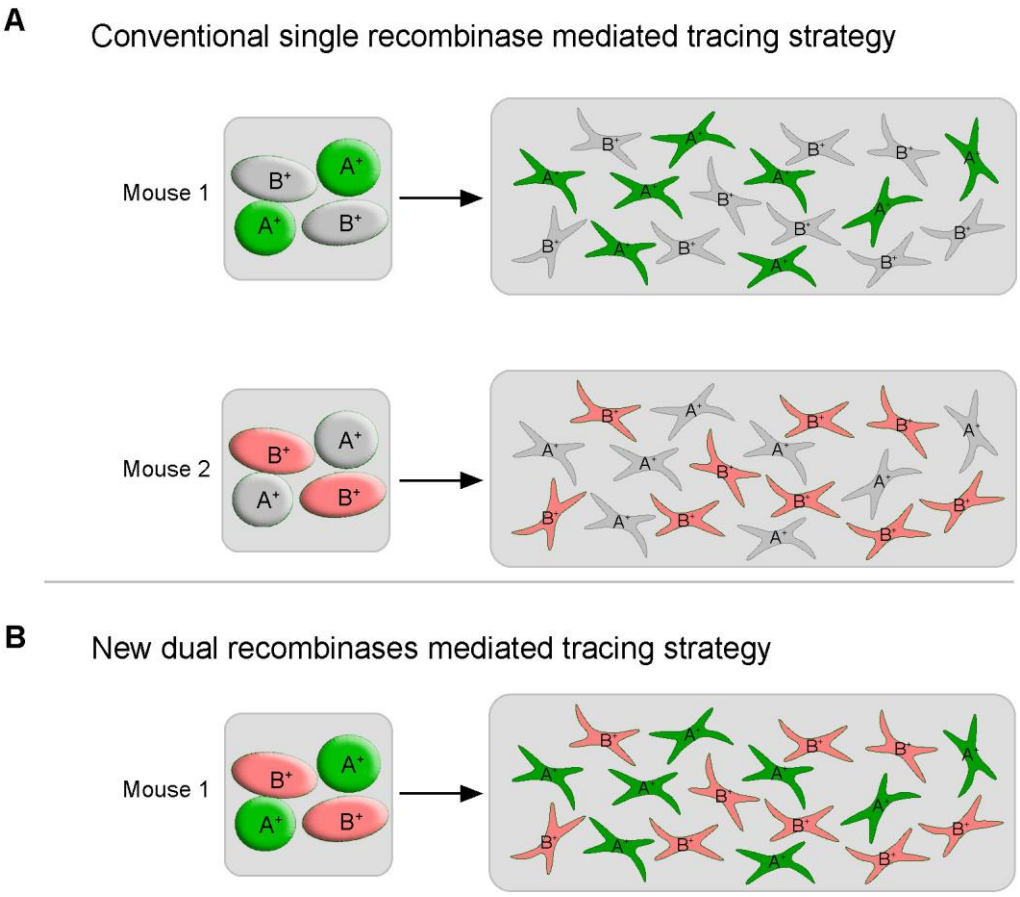

Fig. 6. Comparison of conventional and new lineage tracing strategies. (A) Conventional lineage tracing strategy uses two different promoters that drive Cre recombinases in two different mice for their fate mapping study. (B) In new strategy, both Cre and Nigri recombinases can be driven by two different cell-specific promoters simultaneously within one mouse and allow simultaneous fate mapping of two populations in one mouse.

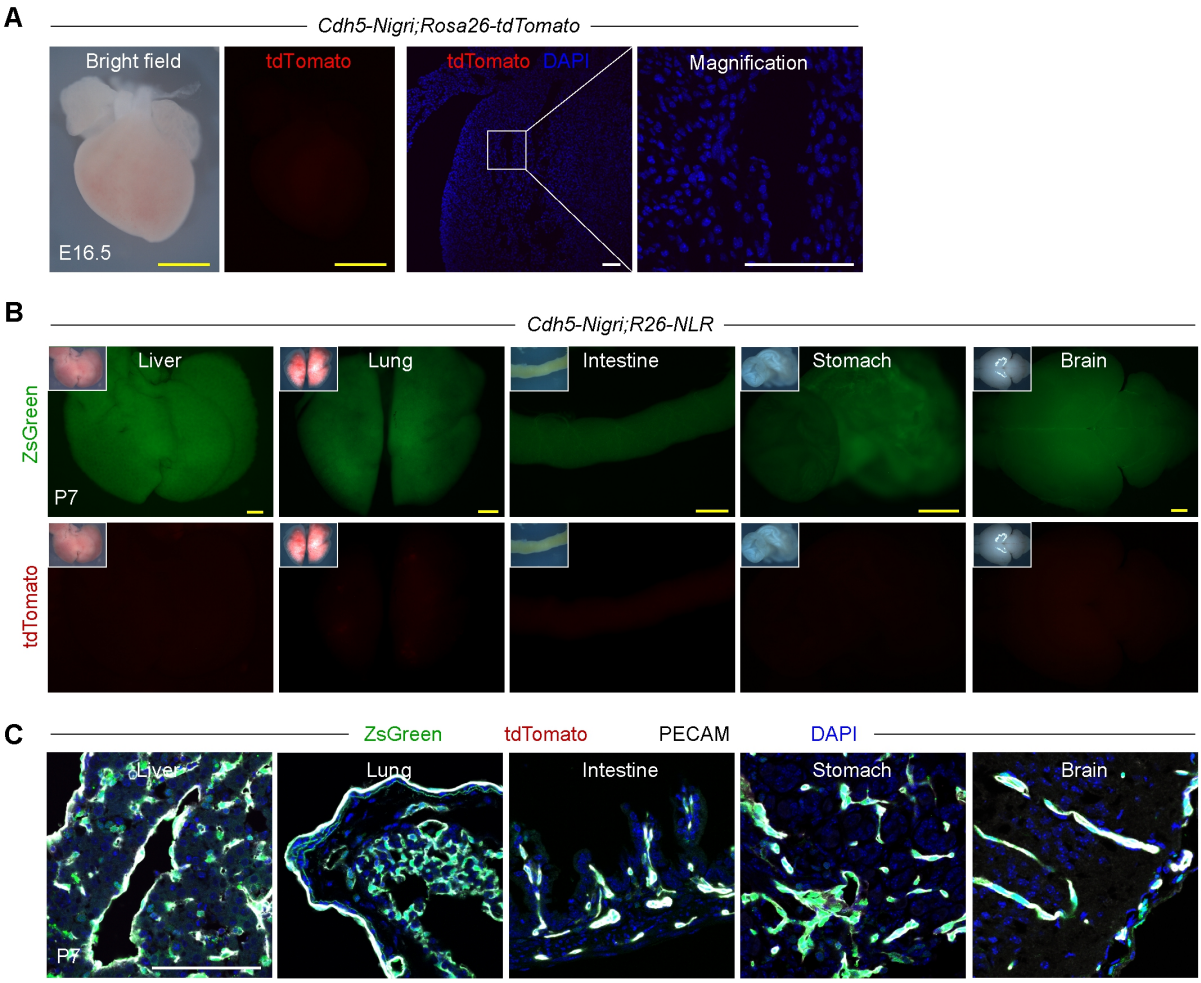

Fig. S1. *Cdh5-Nigri* efficiently and specifically mediated nox sites recombination in endothelial cells *in vivo*. (A) Wholemount views of E16.5 *Cdh5-Nigri;Rosa26-tdTomato* heart. Immunostaining for tdTomato on E16.5 *Cdh5-Nigri;Rosa26-tdTomato* heart shows no cells are tdTomato^{+}. (B) Wholemount views of P7 *Cdh5-Nigri;R26-NLR* organs. (C) Tissues sections from (B) stained for ZsGreen, tdTomato and PECAM shows that PECAM^{+} endothelial cells are ZsGreen^{+}. Yellow bar, 1 mm; white bar, 100 µm. Each image is representative of 4-5 individual biological samples.

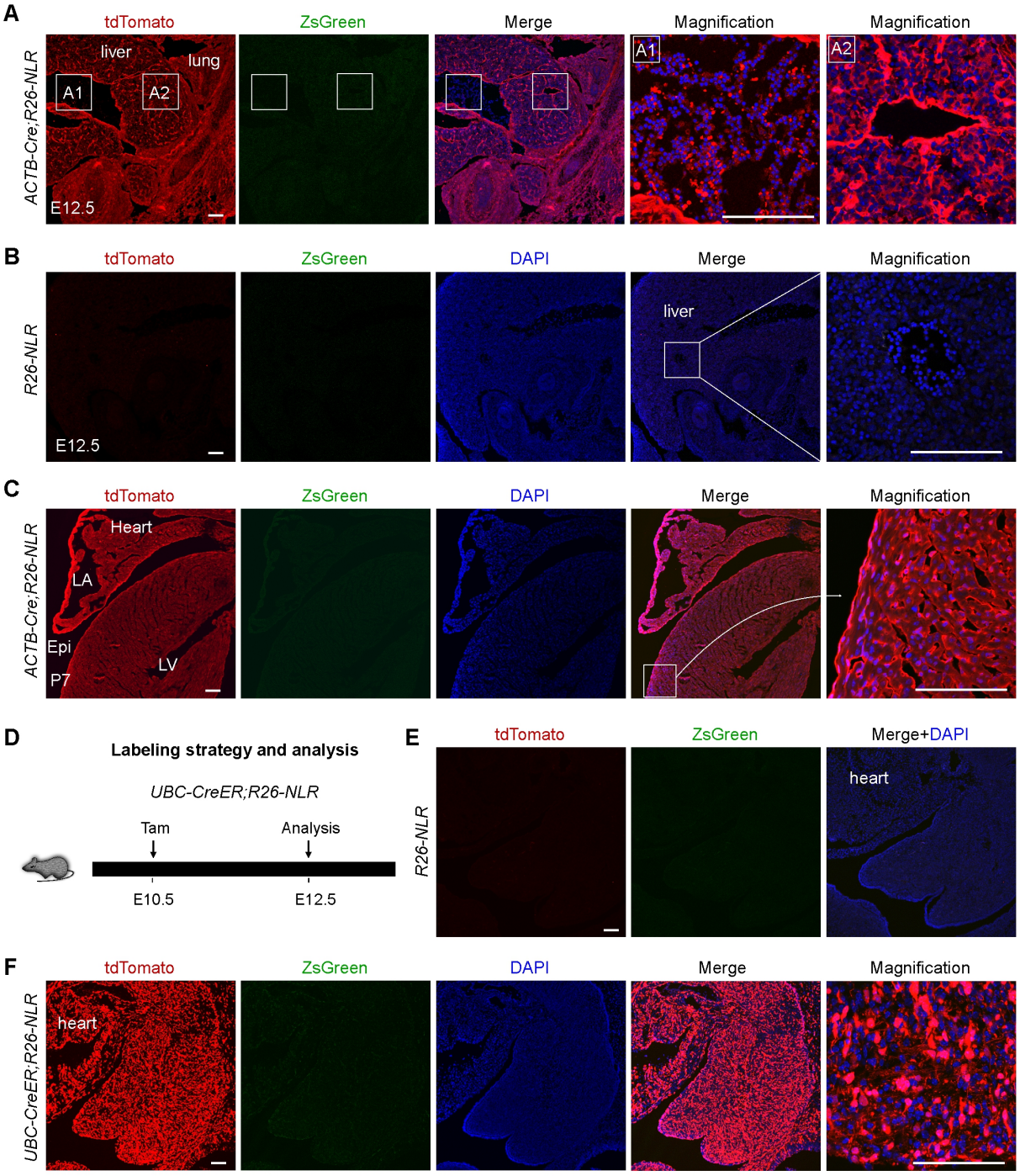

Fig. S2. Cre recombinase efficiently recombines loxP but not nox sites in *R26-NLR* line. (A,B) Immunostaining for ZsGreen and tdTomato on E12.5 *ACTB-Cre;R26-NLR* embryo section shows all cells are tdTomato^{+} (A), and no fluorescent cells in *R26-NLR* embryo (B). (C) Immunostaining for ZsGreen and tdTomato on P7 *ACTB-Cre;R26-NLR* heart section shows all cells are tdTomato^{+}. (D) Schematic image showing experimental strategy. Tamoxifen (Tam) was administered at E10.5 and embryos were collected for analysis at E12.5. (E,F) Immunostaining for ZsGreen and tdTomato on E12.5 *UBC-CreER;R26-NLR* embryo shows all cells are tdTomato^{+} (F), and no fluorescent cells on *R26-NLR* embryo (E). Scale bar, 100 µm. Each image is representative of 4-5 individual biological samples.

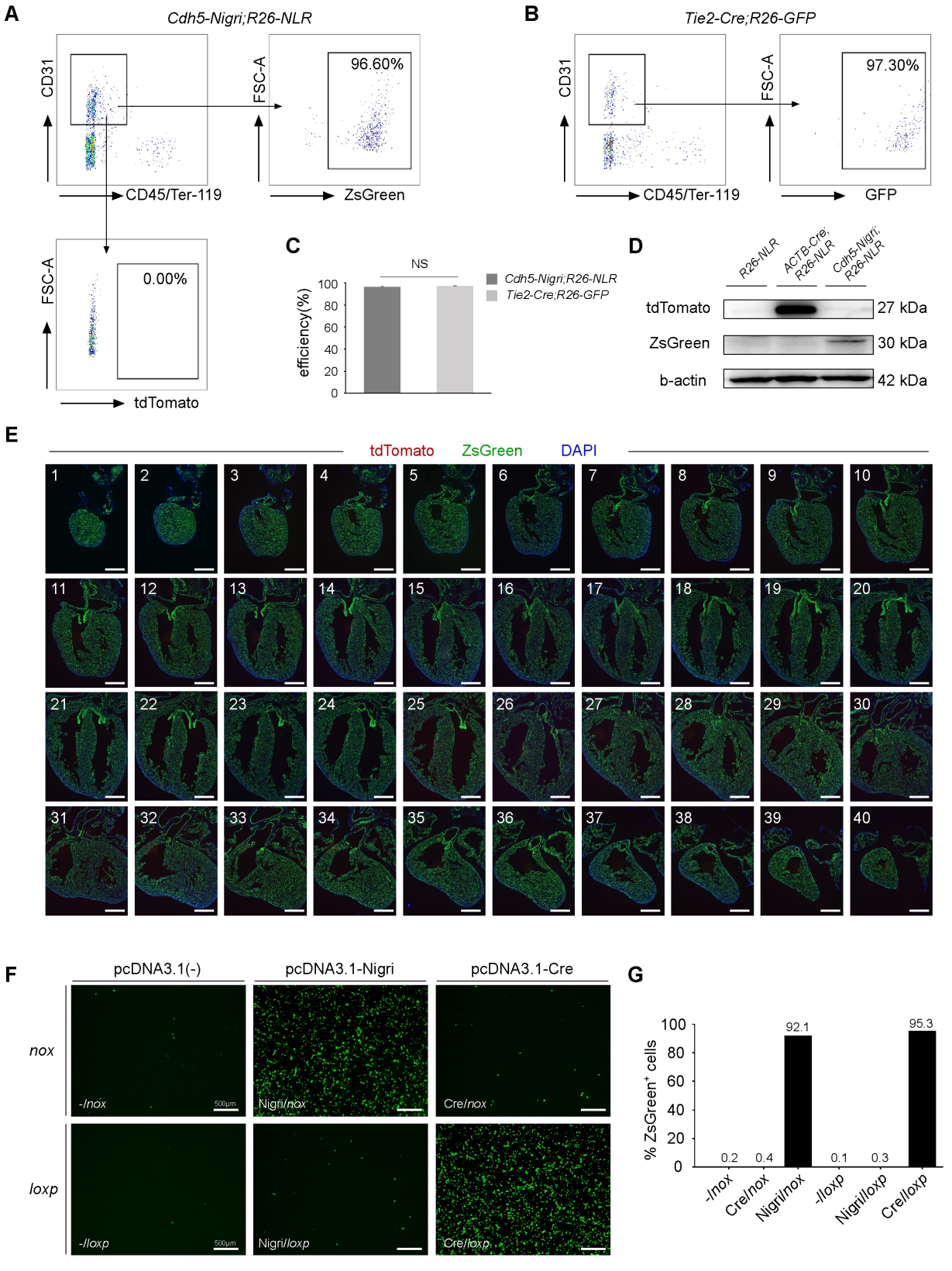

Fig. S3. High efficiency of Nigri-nox and Cre-loxP recombination *in vivo* and negligible crosstalk between Nigri-nox and Cre-loxP systems *in vitro*. (A) Flow cytometric analysis of the percentage of $CD31^+$ endothelial cells labeled by E15.5 *Cdh5-Nigri;R26-NLR* ($ZsGreen^+$) (n=6). (B) Flow cytometric analysis of the percentage of $CD31^+$ endothelial cells labeled by E15.5 *Tie2-Cre;R26-GFP* (GFP^+) (n=6). (C) Quantification results of ZsGreen labeled $CD31^+$ endothelial cells and GFP labeled $CD31^+$ endothelial cells within *Cdh5-Nigri;R26-NLR* and *Tie2-Cre;R26-GFP* tissues. NS, non-significant. (D) Western blot analysis of tdTomato and ZsGreen protein from E15.5 *ACTB-Cre;R26-NLR* and *Cdh5-Nigri;R26-NLR*. *R26-NLR* was used as negative control (n=4). (E) Immunostaining for ZsGreen and tdTomato on serial sections of E15.5 *Cdh5-Nigri;R26-NLR* heart. (F) Recombination analysis between Nigri-nox and Cre-loxP systems after co-transfection of Nigri-expression or Cre-expression plasmids with reporter plasmids. Co-transfections of pcDNA3.1(-) plasmids and reporter plasmids were used as controls. (G) Quantification of recombination efficiency of Nigri-nox and Cre-loxP systems *in vitro* (n=3). Scale bars, 500 μm.

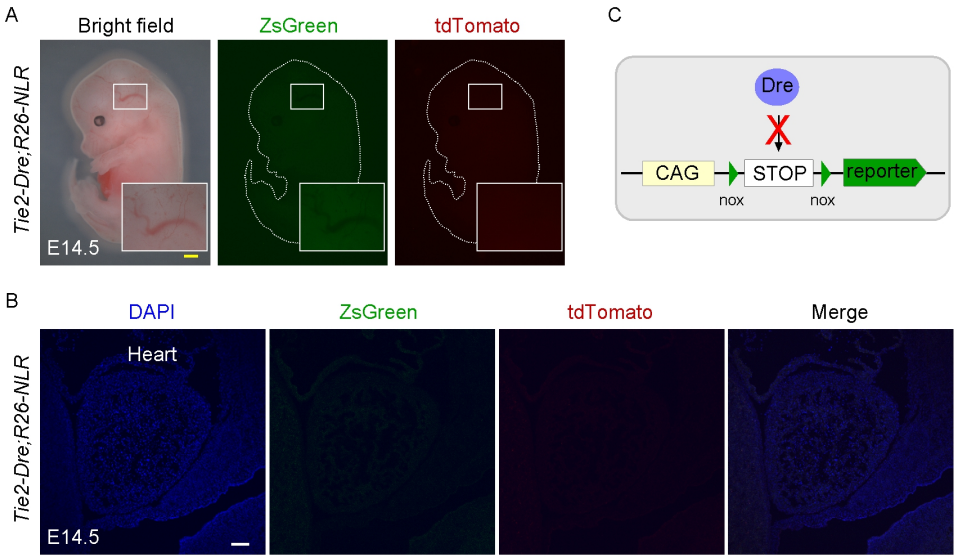

Fig. S4. Dre recombinase can not recombine nox sites in *R26-NLR* line. (A) Wholemount bright-field and epifluorescence views of E14.5 *Tie2-Dre;R26-NLR* embryo. The insets are magnified images of the boxed regions. (B) Immunostaining for ZsGreen and tdTomato on E14.5 *Tie2-Dre;R26-NLR* embryo show no ZsGreen or tdTomato signals detected. (C) Schematic figure showing Dre recombinase can not recognize nox sites in *R26-NLR* line. Yellow bar, 1 mm; white bar, 100 μm. Each image is representative of 4-5 individual biological samples.

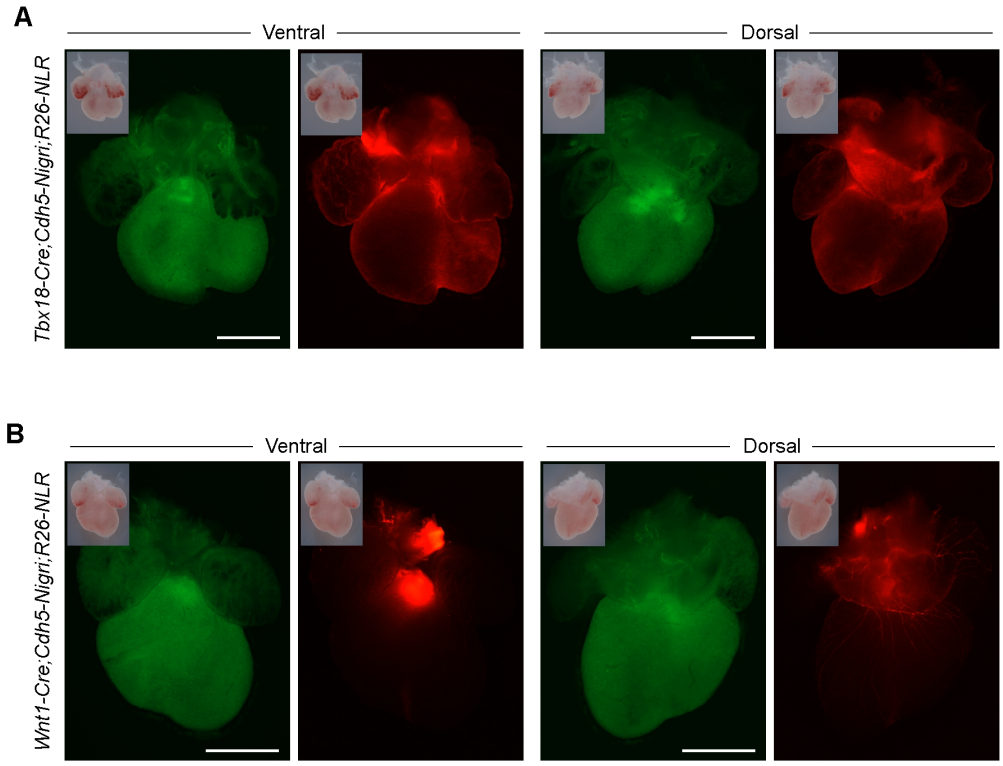

Fig. S5. Simultaneous labeling two genetically distinct progenitor cell populations using *R26-NLR* line. (A) Wholemount views of E14.5 *Tbx18-Cre;Cdh5-Nigri;R26-NLR* embryo showed both expression of tdTomato and ZsGreen in one heart. (B) Wholemount views of E17.5 *Wnt1-Cre;Cdh5-Nigri;R26-NLR* embryo also showed both expression of tdTomato and ZsGreen in one heart. Scale bar, 100 μm. Each image is representative of 4 individual biological samples.

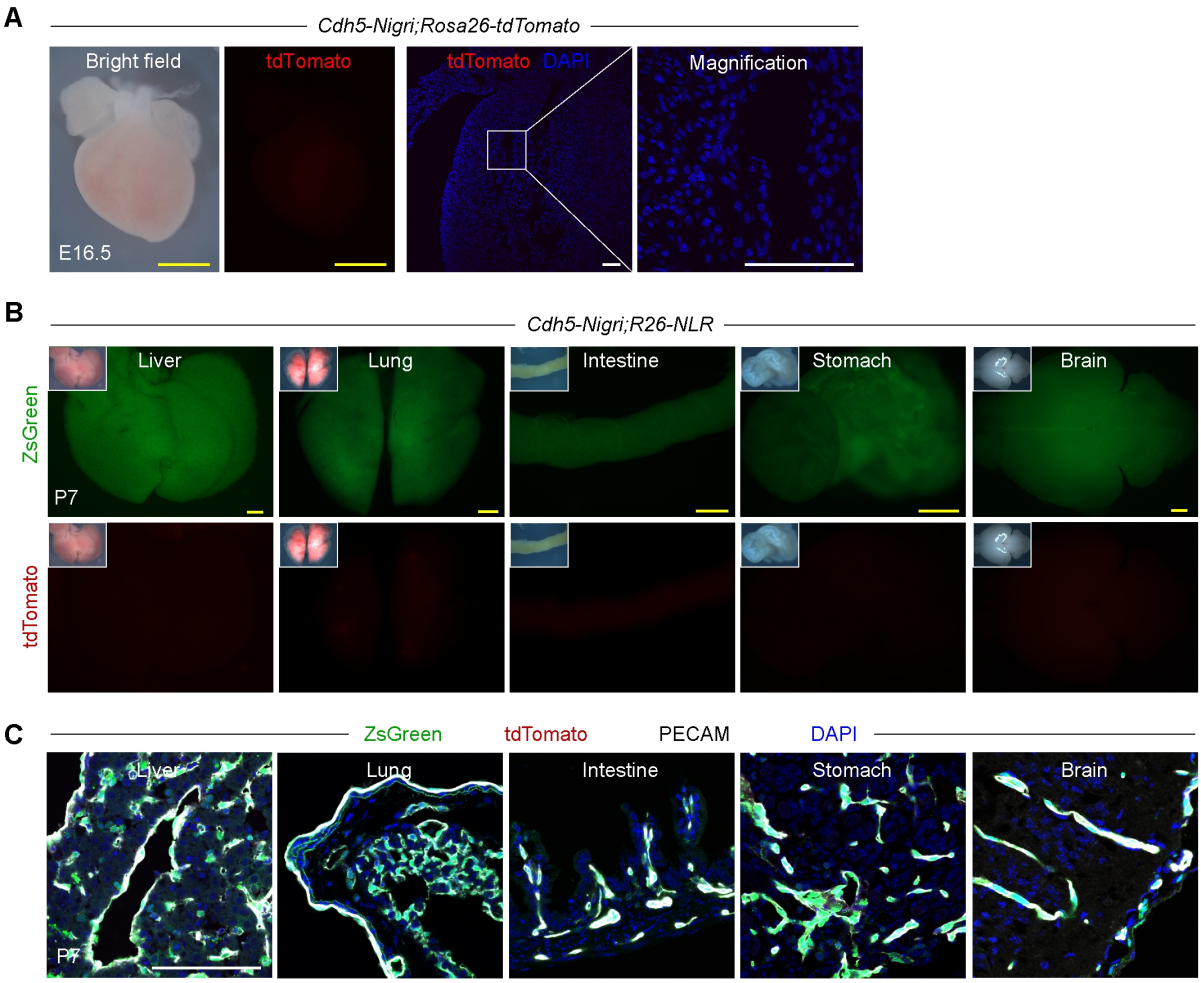

Fig. S1. *Cdh5-Nigri* efficiently and specifically mediated nox sites recombination in endothelial cells *in vivo*. (A) Wholemount views of E16.5 *Cdh5-Nigri;Rosa26-tdTomato* heart. Immunostaining for tdTomato on E16.5 *Cdh5-Nigri;Rosa26-tdTomato* heart shows no cells are tdTomato^{+}. (B) Wholemount views of P7 *Cdh5-Nigri;R26-NLR* organs. (C) Tissues sections from (B) stained for ZsGreen, tdTomato and PECAM shows that PECAM^{+} endothelial cells are ZsGreen^{+}. Yellow bar, 1 mm; white bar, 100 µm. Each image is representative of 4-5 individual biological samples.

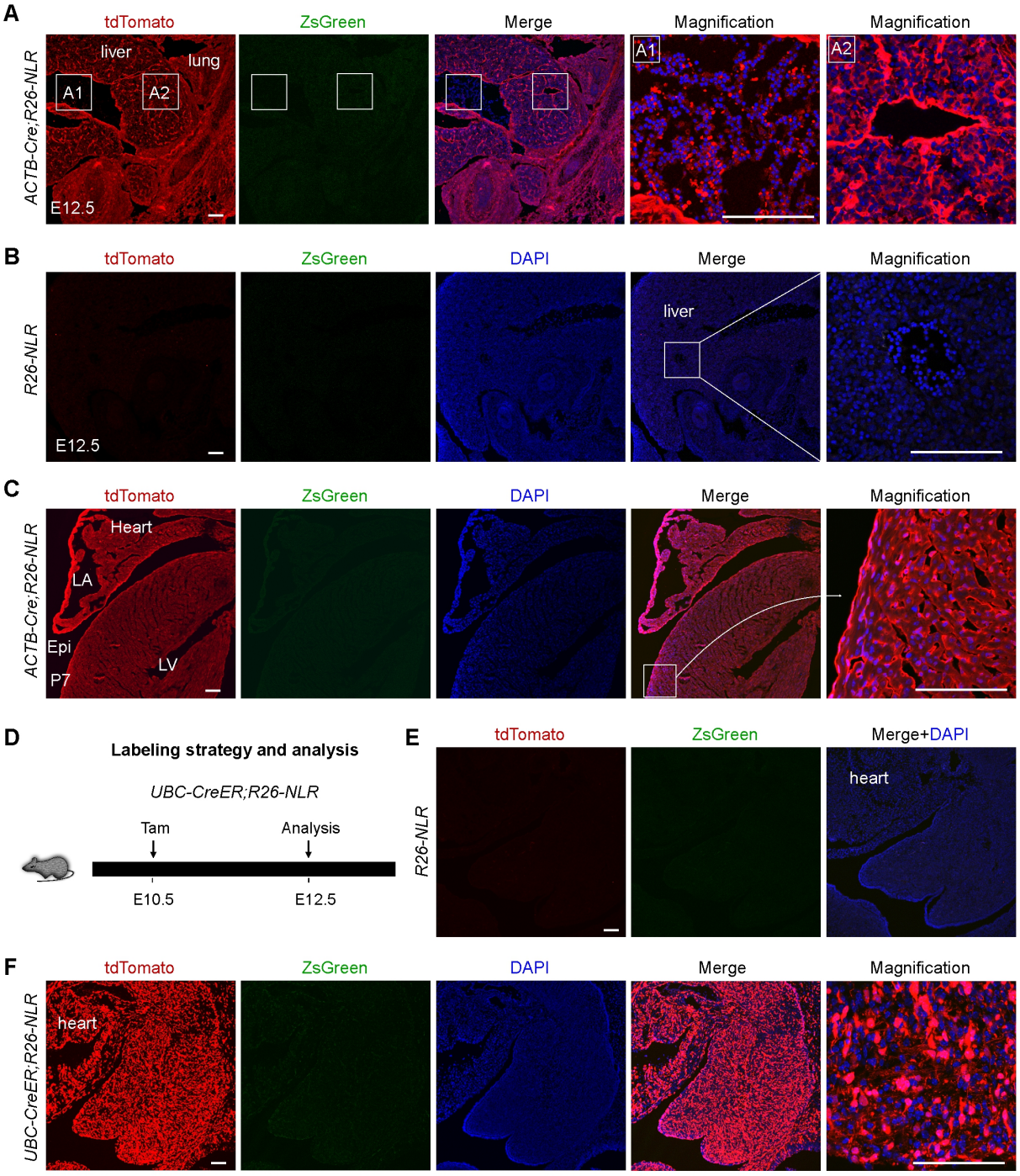

Fig. S2. Cre recombinase efficiently recombines loxP but not nox sites in *R26-NLR* line. (A,B) Immunostaining for ZsGreen and tdTomato on E12.5 *ACTB-Cre;R26-NLR* embryo section shows all cells are tdTomato^{+} (A), and no fluorescent cells in *R26-NLR* embryo (B). (C) Immunostaining for ZsGreen and tdTomato on P7 *ACTB-Cre;R26-NLR* heart section shows all cells are tdTomato^{+}. (D) Schematic image showing experimental strategy. Tamoxifen (Tam) was administered at E10.5 and embryos were collected for analysis at E12.5. (E,F) Immunostaining for ZsGreen and tdTomato on E12.5 *UBC-CreER;R26-NLR* embryo shows all cells are tdTomato^{+} (F), and no fluorescent cells on *R26-NLR* embryo (E). Scale bar, 100 µm. Each image is representative of 4-5 individual biological samples.

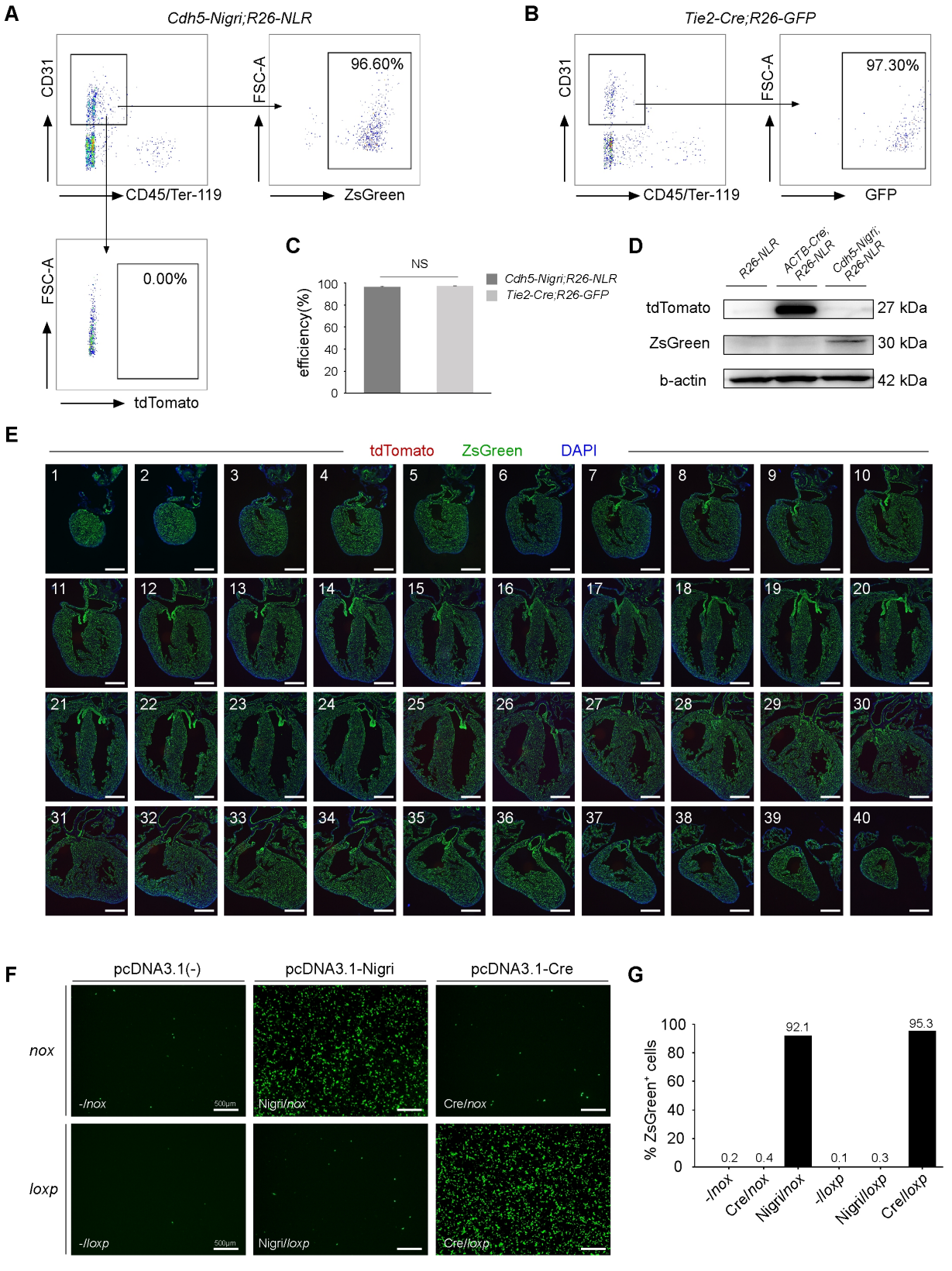

Fig. S3. High efficiency of Nigri-nox and Cre-loxP recombination *in vivo* and negligible crosstalk between Nigri-nox and Cre-loxP systems *in vitro*. (A) Flow cytometric analysis of the percentage of $CD31^+$ endothelial cells labeled by E15.5 *Cdh5-Nigri;R26-NLR* ($ZsGreen^+$) (n=6). (B) Flow cytometric analysis of the percentage of $CD31^+$ endothelial cells labeled by E15.5 *Tie2-Cre;R26-GFP* (GFP^+) (n=6). (C) Quantification results of ZsGreen labeled $CD31^+$ endothelial cells and GFP labeled $CD31^+$ endothelial cells within *Cdh5-Nigri;R26-NLR* and *Tie2-Cre;R26-GFP* tissues. NS, non-significant. (D) Western blot analysis of tdTomato and ZsGreen protein from E15.5 *ACTB-Cre;R26-NLR* and *Cdh5-Nigri;R26-NLR*. *R26-NLR* was used as negative control (n=4). (E) Immunostaining for ZsGreen and tdTomato on serial sections of E15.5 *Cdh5-Nigri;R26-NLR* heart. (F) Recombination analysis between Nigri-nox and Cre-loxP systems after co-transfection of Nigri-expression or Cre-expression plasmids with reporter plasmids. Co-transfections of pcDNA3.1(-) plasmids and reporter plasmids were used as controls. (G) Quantification of recombination efficiency of Nigri-nox and Cre-loxP systems *in vitro* (n=3). Scale bars, 500 μm.

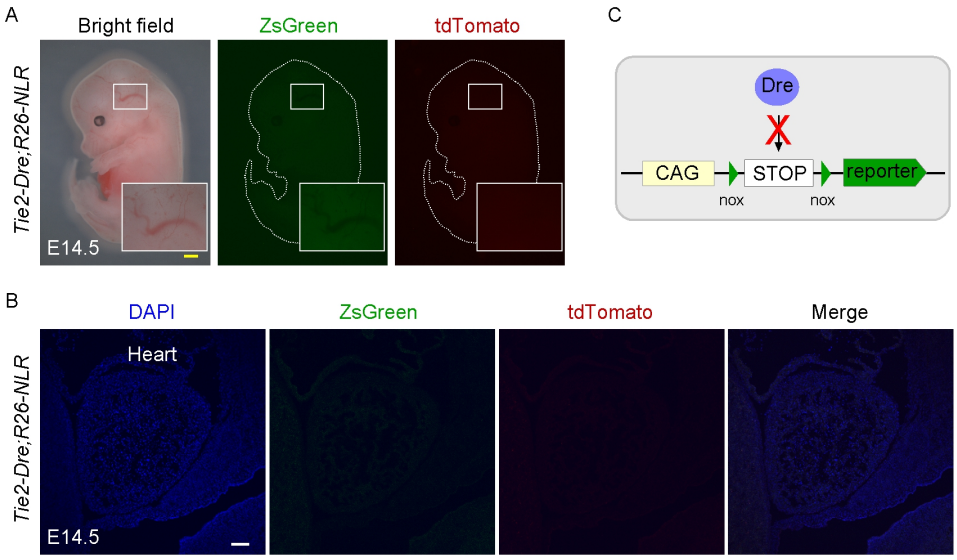

Fig. S4. Dre recombinase can not recombine nox sites in *R26-NLR* line. (A) Wholemount bright-field and epifluorescence views of E14.5 *Tie2-Dre;R26-NLR* embryo. The insets are magnified images of the boxed regions. (B) Immunostaining for ZsGreen and tdTomato on E14.5 *Tie2-Dre;R26-NLR* embryo show no ZsGreen or tdTomato signals detected. (C) Schematic figure showing Dre recombinase can not recognize nox sites in *R26-NLR* line. Yellow bar, 1 mm; white bar, 100 μm. Each image is representative of 4-5 individual biological samples.

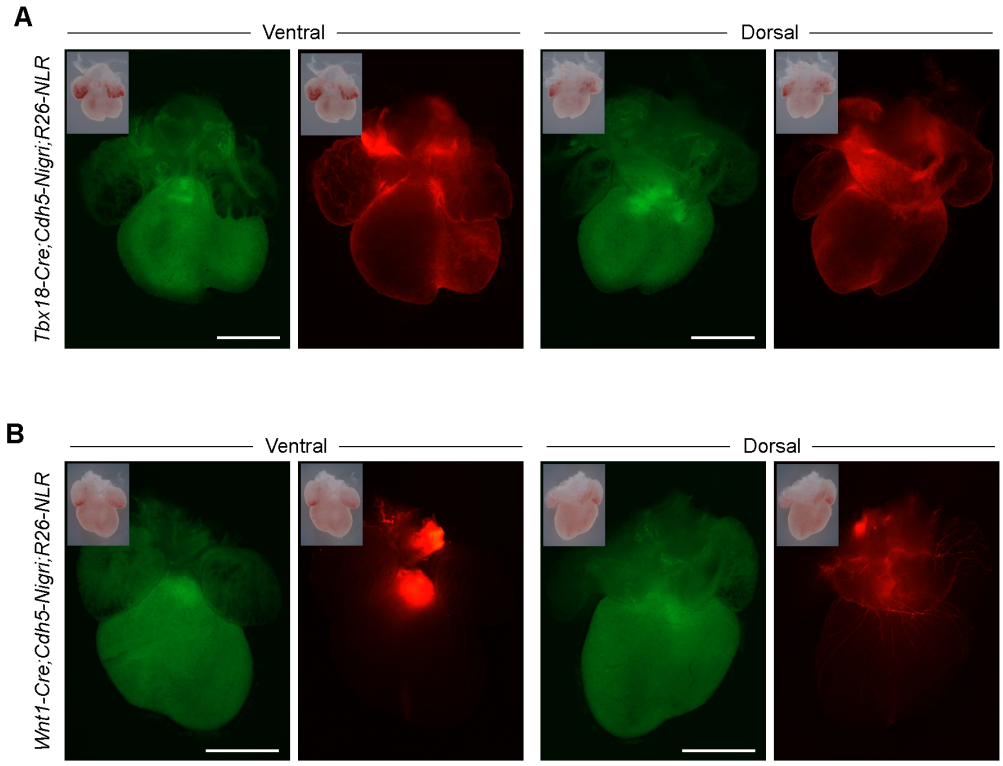

Fig. S5. Simultaneous labeling two genetically distinct progenitor cell populations using *R26-NLR* line. (A) Wholemount views of E14.5 *Tbx18-Cre;Cdh5-Nigri;R26-NLR* embryo showed both expression of tdTomato and ZsGreen in one heart. (B) Wholemount views of E17.5 *Wnt1-Cre;Cdh5-Nigri;R26-NLR* embryo also showed both expression of tdTomato and ZsGreen in one heart. Scale bar, 100 μm. Each image is representative of 4 individual biological samples.